Fungicide Residues Exposure and β-amyloid Aggregation in a Mouse Model of Alzheimer's Disease

Pierre-André Lafon, Yunyun Wang, Margarita Arango-Lievano, Joan Torrent, Lucie Salvador-Prince, Marine Mansuy, Nadine Mestre-Francés, Laurent Givalois, Jianfeng Liu, Josep Vicent Mercader, et al.

A Section 508–conformant HTML version of this article is available at https://doi.org/10.1289/EHP5550.

Fungicide Residues Exposure and β-amyloid Aggregation in a Mouse Model of Alzheimer's Disease

Pierre-André Lafon,[1] Yunyun Wang,[1,2]* Margarita Arango-Lievano,[3] Joan Torrent,[1] Lucie Salvador-Prince,[1] Marine Mansuy,[1] Nadine Mestre-Francès,[1] Laurent Givalois,[1] Jianfeng Liu,[2] Josep Vicent Mercader,[4] Freddy Jeanneteau,[3] Catherine Desrumaux,[1,5] and Véronique Perrier[1]*

[1]MMDN, University of Montpellier, EPHE, INSERM, Montpellier, France
[2]Cellular Signaling Laboratory, College of Life Science and Technology, Huazhong University of Science and Technology, Wuhan, Hubei, China
[3]Institut de Génomique Fonctionnelle, University of Montpellier, CNRS, INSERM, Montpellier, France
[4]Institute of Agrochemistry and Food Technology, Consejo Superior de Investigaciones Científicas (IATA-CSIC), Paterna, València, Spain
[5]LipSTIC LabEx, Fondation de Coopération Scientifique Bourgogne-Franche Comté, Dijon, France

Background: Pesticide residues have contaminated our environment and nutrition over the last century. Although these compounds are present at very low concentrations, their long-term effects on human health is of concern. The link between pesticide residues and Alzheimer's disease is not clear and difficult to establish. To date, no *in vivo* experiments have yet modeled the impact of this chronic contamination on neurodegenerative disorders.

Objectives: We investigated the impact of fungicide residues on the pathological markers of Alzheimer's disease in a transgenic mouse model.

Methods: Transgenic (J20, $hAPP_{Sw/Ind}$) mice were chronically exposed to a cocktail of residues of cyprodinil, mepanipyrim, and pyrimethanil at 0.1 μg/L in their drinking water for 9 months. We assessed the effects of fungicide residues on the pathological markers of the disease including Aβ aggregates, neuroinflammation, and neuronal loss. Then, we studied the dynamics of Aβ aggregation *in vivo* via a longitudinal study using two-photon microscopy. Finally, we investigated the molecular mechanisms involved in the production and clearance of Aβ peptides.

Results: We found that a chronic exposure to three fungicide residues exacerbated aggregation, microgliosis, and neuronal loss. These fungicides also increased vascular amyloid aggregates reminiscent of cerebral amyloid angiopathy between 6 and 9 months of treatment. The mechanism of action revealed that fungicides promoted Aβ peptide fibril formation *in vitro* and involved an *in vivo* overexpression of the levels of the β-secretase–cleaving enzyme (BACE1) combined with impairment of Aβ clearance through neprylisin (NEP).

Conclusions: Chronic exposure of the J20 mouse model of Alzheimer's disease to a cocktail of fungicides, at the regulatory concentration allowed in tap water (0.1 μg/L), strengthened the preexisting pathological markers: neuroinflammation, Aβ aggregation, and APP β-processing. We hypothesize prevention strategies toward pesticide long-term exposure may be an alternative to counterbalance the lack of treatment and to slow down the worldwide Alzheimer's epidemic. https://doi.org/10.1289/EHP5550

Introduction

Alzheimer's disease is the most common form of dementia in elderly people and currently afflicts 50 million people worldwide, and this number is expected to double in the coming generation (OECD 2018). The etiology of Alzheimer's disease has not yet been clarified, which may explain the lack of effective treatments. However, identifying environmental risk factors may represent an alternative strategy to reduce the number of cases. Indeed, projection studies of the incidence of Alzheimer's disease between 2010 and 2050 have indicated that delaying the onset of Alzheimer's disease by 1, 2, or 5 y could decrease its prevalence by about 10%, 20%, and 50%, respectively (Mura et al. 2010).

One of the features of Alzheimer's disease is the accumulation and aggregation of amyloid-β peptides (Aβ) into amyloid plaques (Iwatsubo et al. 1994). Aβ peptides are produced by the sequential enzymatic processing of the amyloid precursor protein (APP) by the β- (BACE1) (Cai et al. 2001; Luo et al. 2001) and γ-secretases (Carroll and Li 2016) (for a review on APP processing, see O'Brien and Wong 2011). Impairments of enzymes such as insulin degrading enzyme (IDE) (Miners et al. 2006, 2009), neprylisin (NEP) (Miners et al. 2009; Zhao et al. 2007), and/or receptors such as the low-density lipoprotein receptor-related protein 1 (LRP1) (Kang et al. 2000; Shinohara et al. 2014) involved in the Aβ clearance pathways are major events reinforcing the disease. The causes leading to these deregulations have not yet been clearly identified. Our hypothesis is that environmental pollutants may corrupt APP metabolism or the Aβ aggregation process, which may lead to the onset or aggravation of Alzheimer's disease.

Human epidemiological studies have showed that circulating levels of certain heavy metals are higher in patients with Alzheimer's disease than in control patients (Fathabadi et al. 2018; Xu et al. 2018). This suggests a potential role of heavy metals in Alzheimer's disease, but it is not yet clear whether they interfere in the development or the progression of the disease. However, experimental studies have showed that incubation of SH-SY5Y cells with lead (5 to 100 μM) can induce an increase of APP expression and Aβ peptides secretion, associated with a decreased NEP expression (Chin-Chan et al. 2015; Huang et al. 2011). Furthermore, an acute injection of lead [27 mg/kg via the intraperitoneal (ip) route] in a mouse model of Alzheimer's disease (APP V717F) has resulted in a lower expression of LRP1 in the choroid plexus than injection of vehicle (Gu et al. 2011). Mercury was shown to be involved in the disruption of Aβ peptide clearance pathways both *in vivo* [in rats: 2 mg/kg per day for 4 weeks by gavage (Kim et al. 2014)] and *in vitro* [in SH-SY5Y cells: 10 and 20 μM (Chin-Chan et al. 2015)]. Moreover, rats orally treated with aluminum (20 g/d, twice a week) through diet, from 6 months of age until the end of their life and who developed cognitive deficits, presented an

*These authors contributed equally to this work.
Address correspondence to Véronique Perrier, MMDN, University of Montpellier, EPHE, INSERM, Place Eugène Bataillon, CC105, 34095 Montpellier Cedex 05, France. Telephone: 33 4 67 14 33 87. Email: Veronique.perrier@umontpellier.fr

Supplemental Material is available online (https://doi.org/10.1289/EHP5550).
The authors declare they have no actual or potential competing financial interests.
Received 30 April 2019; Revised 12 December 2019; Accepted 13 December 2019; Published 15 January 2020.

up-regulation of the APP gene and a greater APP accumulation in hippocampal and cortical neurons compared with cognitively intact control rats (Walton and Wang 2009). *In vitro* treatment with aluminum (50 μM) on rat cortical neurons revealed Aβ peptides conformational changes and enhanced aggregation (Kawahara et al. 2001). Regarding pesticides, occupational exposure of farmers to organophosphates has been associated with an increased risk to develop Alzheimer's disease (Hayden et al. 2010). Moreover, in their clinical study Richardson et al. (2014) found a 4-fold higher level of dichlorodiphenyldichloroethylene (DDE), a metabolite of the organochlorine insecticide dichlorodiphenyltrichloroethane (DDT), in the serum of Alzheimer's disease patients compared with controls. Among these patients, the apolipoprotein E ε4 (APOE4) carriers with higher DDE levels had lower mini-mental state (MMS) scores (Richardson et al. 2014).

Although herbicides and insecticides have been highlighted for their role in Alzheimer's disease, data on the impact of fungicides in neurological disorders have barely been reported. Fungicides are widely used for the cultivation and preservation of fresh fruits and vegetables. Because prevention campaigns encourage people to consume fruits and vegetables every day, we wonder if long-term exposure to fungicide residues, present in these foodstuffs, can affect human health. In this study, we focused our attention on three widely used fungicides: cyprodinil (cypro), mepanipyrim (mepa), and pyrimethanil (pyri), belonging to the anilinopyrimidine class. Many reports and publications have underlined the presence of anilinopyrimidine residues throughout our environment: in the air (ANSES 2010; Désert et al. 2018), in soils (Bermúdez-Couso et al. 2007; Rial-Otero et al. 2004), and in water (ANSES 2013; Herrero-Hernández et al. 2016) (Table 1). Several French (ANSES 2011) and European (EFSA 2017b, 2018, 2019) reports have showed that residues of cypro, mepa, and pyri were detected in many foodstuffs, findings that have been confirmed by studies from independent nongovernmental organizations (Générations Futures 2013, 2016a; PAN Europe 2008) (Table 1). From an epidemiological standpoint, it is difficult to assess the impact of a long-term exposure to pesticide residues on neurodegenerative diseases such as Alzheimer's disease. Indeed, the majority of Alzheimer's disease cases are diagnosed in elderly populations, yet the exposure to risk factors occur years or decades before the first symptoms appear. However, one can hypothesize that chronic exposure to pesticide residues via our diet or drinking water may have a role in the etiology or aggravation of neurological diseases.

To test this hypothesis, we investigated the impact of fungicide residues on the J20 mouse model of Alzheimer's disease ($hAPP_{Sw/Ind}$) (Mucke et al. 2000). Mice were chronically exposed to a cocktail of cypro, mepa, and pyri at the regulatory limit dose of 0.1 μg/L for each compound over 9 months through tap water. We analyzed different markers of Alzheimer's disease such as soluble and aggregated Aβ peptides, astrogliosis, microgliosis, and neuronal loss. To better understand the dynamics of aggregation with the cocktail of fungicides, we performed a longitudinal study at 3, 6, and 9 months posttreatment using two-photon microscopy. To decipher the impact of these fungicides on either the amyloidogenic or the clearance pathways, we analyzed the main proteins involved (i.e., APP, BACE1, NEP, IDE, LRP1). The potential interaction of anilinopyrimidines with the different forms of Aβ was analyzed through *ex vivo* binding experiments and *in vitro* kinetics of amyloid fibril formation.

Materials and Methods

Animals Used and Breeding

This project followed the specific French national guidelines on animal experimentation and well-being and was approved by the French National Ethics Committee for Animal Experimentation (APAFIS no. 7357-20161025-18055782). Hemizygous $hAPP_{Sw/Ind}$ transgenic mice (referred to as $hAPP^{+/+}_{Sw/Ind}$ or also called J20 mice) (Mucke et al. 2000) were purchased from Jackson

Table 1. Occurrences and C_{max} of cyprodinil, mepanipyrim, and pyrimethanil residues in the European diet and environment.

Elements analyzed	Cyprodinil	Mepanipyrim	Pyrimethanil	References
Fruits	37.3% ($n=75$) C_{max}: 90 μg/kg[a]	6.7% ($n=75$) C_{max}: 40 μg/kg	17.3% ($n=75$) C_{max}: 320 μg/kg	ANSES 2011
Vegetables	18.7% ($n=267$) C_{max}: 480 μg/kg	No data	12.7% ($n=267$) C_{max}: 180 μg/kg	ANSES 2011
Strawberries	29.5% ($n=61$) C_{max}: 1.6 mg/kg	1.6% ($n=61$) C_{max}: <LOQ	0% ($n=61$)	Générations Futures 2013
Breakfast cereals	73.33% ($n=15$) C_{max}: 36 μg/kg	No data	100% ($n=15$) C_{max}: 140 μg/kg	Générations Futures 2016a
Table grapes	16.00% ($n=1,287$)[b]	No data	9.52% ($n=1,187$)[b]	EFSA 2017a
Strawberries	34.49% ($n=1,206$)[b]	6.97% ($n=1,206$)[b]	7.21% ($n=1,206$)[b]	EFSA 2018
Pears	11.09% ($n=1,199$)[b]	No data	7.42% ($n=1,199$)[b]	EFSA 2019
Water (La Rioja, Spain)	C_{max}: 0.981 μg/L	No data	C_{max}: 0.59 μg/L	Herrero-Hernández et al. 2016
Austrian wine	71.4% ($n=7$) C_{max}: 15 μg/kg	No data	85.7% ($n=7$) C_{max}: 48 μg/kg	PAN Europe 2008
French wine	50% ($n=10$) C_{max}: 6.8 μg/L	No data	90% ($n=10$) C_{max}: 233.8 μg/L	PAN Europe 2008
German wine	18.2% ($n=11$) C_{max}: 10 μg/kg	No data	63.6% ($n=11$) C_{max}: 190 μg/kg	PAN Europe 2008
Dust	86.4% ($n=22$) C_{max}: 372.3 ng/g	9.1% ($n=22$) C_{max}: <LOQ	68.2% ($n=22$) C_{max}: 21.4 ng/g	Générations Futures 2016b
Hair	14.3% ($n=7$) C_{max}: <LOQ	No data	57.1% ($n=7$) C_{max}: <LOQ	Générations Futures 2017
Atmosphere	25% ($n=1,515$) C_{max}: 35.9 ng/m^3	No data	No data	ANSES 2010

Note: C_{max}, maximal concentration; LOD, limit of detection; LOQ, limit of quantification.
[a]C_{max}: maximal concentrations measured in the referred studies.
[b]Occurrences were calculated according to the total number of samples analyzed and the number of samples presenting residues of pesticides in quantified concentrations (above the LOQ; >0.1 μg/kg). However, samples with pesticide residues below the LOD (0.03 μg/kg) were not reported in these studies because the reporting countries of the European Union did not compile the information consistently. So, samples were not taken into account when residues concentration was below the LOQ.

Laboratories. A material transfer agreement (no. UM140255-01) was signed with the Gladstone Institute for the use of the J20 mice. All the mice used were on a C57BL/6J background and were backcrossed >10 generations. Then, $hAPP^{+/-}_{Sw/Ind}$ mice were mated between them in order to obtain $hAPP^{+/+}_{Sw/Ind}$ mice (25% of the colony). Wild-type (WT) animals ($hAPP^{-/-}_{Sw/Ind}$) were issued from the same litter (25% of the colony) and were used as controls. To obtain the number of animals sufficient for this study, we used at least 15 breeding cages; each of them containing 3 females and 1 male $hAPP^{+/-}_{Sw/Ind}$. Pregnant mice were separated in individual cages until weaning of their offspring. Genotyping of mice was performed as described by Mansuy et al. (2018) and Mucke et al. (2000). Due to the low percentage of $hAPP^{+/+}_{Sw/Ind}$ and WT mice generated, the different groups were established from different female mice, with a maximum of five animals per cage. Animals were housed under 12-h light/12-h dark cycle, at 23 ± 2°C and 53 ± 10% of relative humidity. Animals had free access to water and food and were fed a standard chow diet (A03, SAFE Diets).

The J20 mouse model overexpresses human APP containing the Swedish (K670N/M671L) and Indiana (V717F) mutations under the control of platelet-derived growth factor-beta (PDGF-β) promoter, leading to a neuronal expression of the transgene (Mucke et al. 2000). This model overproduces $A\beta_{1-42}$ peptides. The appearance of aggregates is progressive, with robust plaques in the hippocampus and the cortex by 8–9 months of age (Mucke et al. 2000). This mouse model does not exhibit neurofibrillary tangles (Mucke et al. 2000). J20 mice exhibit a neuronal loss at 3, 6, and 9 months of age in the CA1 area of the hippocampus but not in the CA3 area (Wright et al. 2013). Regarding astrogliosis, a significant increase of glial fibrillary acidic protein (GFAP)–positive cells was observed in the hippocampus of J20 mice at 6 and 9 months of age compared with age-related WT mice (Wright et al. 2013).

Animals' Treatment and Experiments

Cypro, mepa, and pyri were purchased from Sigma-Aldrich. Stock solutions were prepared in glass vials (Wheaton) at 1 mg/mL in pure dimethyl sulfoxide (DMSO) according to the supplier's recommendations. Stock solutions were diluted 1,000 times in distilled water to a final concentration of 1 mg/L, filtered (0.5 μm), and stored in glass bottles (Duran-Schott) at 4°C until use. For animal treatment, stock solutions at 1 mg/L were further diluted 10,000 times in tap water to reach a final concentration of 0.1 μg/L. Animals' treatment started after weaning (at postnatal day 30), and they were treated with a cocktail of the three fungicides at 0.1 μg/L each (cypro: 444 pM; mepa: 448 pM; and pyri: 502 pM) (Figure 1A), which corresponds to the regulatory maximal limit dose allowed in drinking water (Council of the European Union 1998). According to EU regulations, the total concentration of several pesticide residues in drinking water cannot exceed 0.5 μg/L (Council of the European Union 1998). In parallel, a solution of pure DMSO (100%) was diluted 1,000 times in distilled water to a final concentration of 0.1%, filtered (0.5 μm), and stored in a glass bottle at 4°C until use. To treat control vehicle animals, the stock solution of DMSO at 0.1% was further diluted 10,000 times in tap water (1×10^{-5} % corresponding to the equivalent volume of one fungicide). Thus, for three fungicides, the final percentage of DMSO is 3×10^{-5}. Mice water bottles were changed once a week for all groups and prepared from stock solutions as described above. Each week, water levels were measured for each cage and pesticide consumption was estimated per mouse. In parallel, the body weight gain was measured every month.

For this project, a total of 33 J20 and 31 WT mice were treated with the cocktail of the three fungicides via the drinking water (referred to as T groups) for 9 months (35 weeks) after weaning (Figure 1B). Control groups (J20 $n = 32$ and WT $n = 30$) were treated with an equivalent volume of DMSO and referred to as CTR groups (Figure 1B). All these mice were generated from three independent breedings. Animals obtained from the first set of experiments, referred to as Study 1 (WT CTR: $n = 27$; WT T: $n = 28$; J20 CTR: $n = 25$; and J20 T: $n = 24$), were used for biochemical analyses (left hemispheres for $A\beta_{1-42}$ assay) and for immunohistochemistry [right hemispheres for thioflavin T (ThT) staining and detection of fungicides] (Figure 1C, Study 1). A second breeding, called Study 2 (WT CTR: $n = 3$; WT T: $n = 3$; J20 CTR: $n = 4$; and J20 T: $n = 4$) was done to perform *a*) the labeling with the anti-GFAP, anti-ionized calcium binding adaptor molecule 1 (IBA1), and anti-neuronal nuclei (NeuN) antibodies; *b*) for interleukins (ILs) and cytokines time resolved–fluorescence resonance energy transfer (TR-FRET, also called homogeneous time resolved fluorescence or HTRF® assays); *c*) quantitative polymerase chain reaction (qPCR) analyses; and *d*) western blotting (Figure 1C, Study 2). Mice from a third experiment, called Study 3 (J20 CTR: $n = 3$ and J20 T: $n = 5$), were used in a longitudinal study of appearance of plaques using two-photon microscopy at 3, 6, and 9 months posttreatment (Figure 1D). In addition, six 10-month-old J20 mice (without any treatment) were used for *ex vivo* interaction assays of fungicides with amyloid plaques. Detailed protocols of these experiments are described below.

Tissue Collection and Preparation

After 9 months of treatment, mice from Studies 1 and 2 were anesthetized [16% ketamine, 4% xylazine in sodium chloride (NaCl) 0.9%] and sacrificed by a cardiac perfusion of phosphate-buffered saline (PBS), to remove blood from tissues. Brains were removed and cut along the sagittal axis: The left hemispheres were frozen directly in liquid nitrogen and stored at −80°C (for biochemical analyses), and the right hemispheres were fixed in a commercial paraformaldehyde solution (AntigenFix, Diapath) for 48 h at 4°C (for immunohistochemistry). Right hemispheres were rinsed with PBS and incubated in a 30% sucrose solution for 4 d at 4°C. Brains were then included in optimum cutting temperature compound (Tissue-Tek® O.C.T.; Sakura Finetek), quickly frozen in acetone chilled on dry ice, and conserved at −80°C until use.

Ex Vivo *Interaction of Cypro, Mepa, and Pyri with Amyloid Plaques on J20 Brain Tissue Sections*

Frozen brains included in OCT from 6 J20 mice, without any treatment, were mounted on a cryostat (Leica) and 25-μm coronal sections were performed and conserved at −20°C in an antifreeze solution (25% glycerol and 25% ethylene glycol in 0.1 M phosphate buffer) until use. Three to six brain sections per mouse were rinsed, mounted on Superfrost™ Plus glass slides (Microm), and then dried overnight at room temperature (RT). Prior to amyloid labeling, tissue sections were incubated for 10 min with a 70% formic acid solution for antigen retrieval. Sections were then washed in PBS and incubated 1.5 h at RT with a solution containing 2 mM of cypro, or mepa, or pyri or a cocktail of the three fungicides (2 mM each). Sections were incubated 1 h at RT with a blocking solution (3% goat serum, 0.3% Triton X100 in PBS) and then 2 h at RT with a mouse anti-β-amyloid 1-16 conjugated to AlexaFluor® 488 (1:1,000, clone 6E10, Ozyme; referred to as 6E10-Alexa488), followed with the primary antibodies recognizing cypro (Esteve-Turrillas et al. 2012), mepa (Esteve-Turrillas et al. 2013), or pyri (Mercader et al. 2012). Then, the sections were incubated with a goat anti-mouse Cy3 antibody (Jackson ImmunoResearch) for 2 h at RT, and sections were counterstained with 2-(4-amidinophenyl)-1*H*-indole-6-carboxamidine (DAPI; 1:50,000 in PBS) (Molecular Probes). To test the

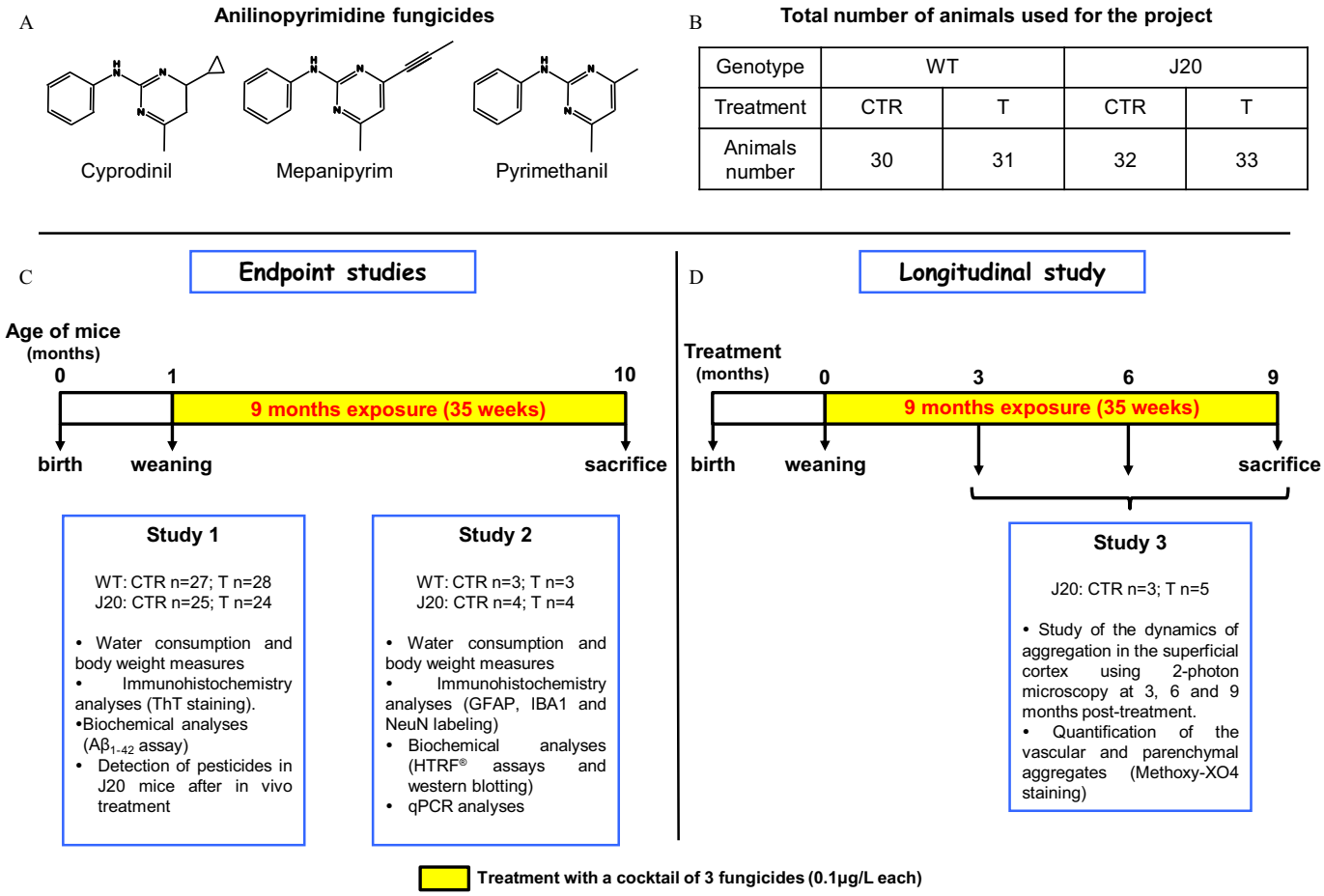

Figure 1. (A) Chemical structure of the three fungicides, (B) total number of animals used for the project, and schematic overviews of (C) treatments and analyses of end point and (D) longitudinal studies. (A) Chemical structures of cyprodinil, mepanipyrim, and pyrimethanil exhibiting fungicide properties. (B) Total number of WT and J20 mice treated with a cocktail of cyprodinil, mepanipyrim, and pyrimethanil (0.1 µg/L each) (T) or with an equivalent volume of DMSO (3×10^{-5} %) (CTR), for 9 months. (C) Study design schema of the end point studies. Weaned WT and J20 mice were treated with fungicides or DMSO, during 9 months (35 weeks), in two independent studies. Study 1 and Study 2 were used to measure water consumption, and body weight and to perform immunohistochemistry, biochemical, and qPCR analyses. (D) Study design schema of the longitudinal study, referred to as Study 3. Weaned J20 mice were treated with fungicides or DMSO, during 9 months and two-photon analyses were done at 3, 6, and 9 months posttreatment on the same animals to evaluate the dynamics of Aβ aggregation. Note: CTR, control; DMSO, dimethyl sulfoxide; GFAP, glial fibrillary acidic protein; HTRF®, homogeneous time resolved fluorescence; IBA1, ionized calcium binding adaptor molecule 1; NeuN, neuronal nuclei; qPCR, quantitative polymerase chain reaction; T, treatment; ThT, thioflavin T; WT, wild type.

specificity of the anti-fungicide antibodies, control brain tissue sections were incubated either with PBS or with an equivalent volume of DMSO (1%) corresponding to the final concentration present in the cocktail of fungicides used. Then, control slides were incubated either without any anti-fungicide antibodies or with secondary antibody Cy3 alone, or anti-fungicide antibodies (anti-cypro, -mepa, and -pyri) alone or in cocktail. All slides were revealed with a goat anti-mouse Cy3 antibody as described above, excepted for the control slide without any fungicide antibodies. All images were taken with a Leica DM2500 microscope (Leica Microsystems) (magnifications: ×20 and ×40).

Kinetics of Fibril Formation of Human $A\beta_{1-42}$ Peptides in Presence of a Cocktail of Cypro, Mepa and Pyri

Synthetic human $A\beta_{1-42}$ peptides were purchased from the ERI Amyloid Laboratory LLC. Peptides were maintained in a monomeric state using the protocol described by Serra-Batiste et al. (2016). Briefly, Aβ peptides were dissolved in a 6.8 M guanidine thiocyanate solution (Sigma-Aldrich) at a concentration of 8.5 mg/mL. The solution was then sonicated for 5 min at 52°C and diluted with ultrapure water to reach a final concentration of 5 mg/mL of Aβ peptides and 4 M of guanidine thiocyanate. The solution was centrifuged at 10,000 × *g* for 6 min at 4°C. The collected supernatant was filtered [polyvinylidene fluoride (PVDF); 0.45 µm] and then injected into a Superdex® 75 Increase 10/300 GL column (GE Heathcare Life Science) previously equilibrated with 10 mM sodium phosphate buffer at pH 7.4. Purification was performed with a 0.5-mL/min flow to collect the peak attributed to monomeric Aβ peptides. Then, their concentration was determined with a NanoDrop™ 8,000 spectrophotometer (Thermo Scientific), and aliquots of peptides were stored at −20°C. The Aβ stock solution was diluted to 30 µM in a 10 mM sodium phosphate buffer at pH 7.4 and left to aggregate in low-binding Eppendorf tubes with a final volume of 600 µL. Experiments with a cocktail of the three fungicides were conducted under the same conditions, except that fungicides were added from a filtered (PVDF; 0.22 µm) stock solution to get a 1:1 or 1:15 M ratio (Aβ:fungicides), with a final concentration of DMSO of 1% (vol/vol) for both conditions. To keep the conditions identical in the control tubes, an equivalent volume of DMSO was added. Each condition was performed in duplicate. Tubes arranged vertically were incubated at 25°C under quiescent state. Fibril formation was monitored by a ThT binding assay. Briefly, 20-µL aliquots were withdrawn at specific times

and mixed with 14 µL of 142 mM Glycine-sodium hydroxide (GlyNaOH) buffer at pH 8.3 and 6 µL of 100 µM of ThT, in a 96-well plate of black polystyrene with clear bottoms and a polyethylene glycol coating (Thermofisher Scientific). ThT fluorescence of each sample was measured ($\lambda_{ex} = 445$ nm and $\lambda_{em} = 485$ nm) in a Fluoroskan Ascent™ microplate fluorimeter (Thermofisher Scientific). Aggregation profiles were generated with GraphPad Prism software (version 5.0; GraphPad), and each kinetic trace was fitted independently using the built-in sigmoidal fit.

Aggregate Staining and Quantification

For this experiment, the number of brains analyzed per group was as follows: WT CTR: $n = 4$; WT T: $n = 4$; J20 CTR: $n = 7$; and J20 T $n = 8$ (Figure 1C, Study 1). Floating brain tissue sections were incubated with ThT, a fluorescent dye, used to stain amyloid plaques. Sections were first mounted on Superfrost® Plus glass slides, dried overnight at RT, incubated with a ThT solution at 0.01% (31 µM) for 10 min (Sigma-Aldrich), rinsed with an 80% ethanol solution and counterstained with DAPI (1:50,000) (Molecular Probes). All sections were visualized under a Leica DM2500 microscope (Leica Microsystems) (magnifications: ×20 and ×40 for enlargements). Images were analyzed with Fiji software (version 2.0; National Institutes of Health). Hemi-brain tissue sections were used to quantify the number and the surface area of amyloid aggregates in the hippocampus and the cortex. Eight to 10 sections were used per animal, and all the values obtained were pooled to get the total number and total surface area of aggregates for each region analyzed. These data were then normalized to the animal's total surface area of hippocampus or cortex of the section quantified. In parallel, the distribution of amyloid plaques within the different regions of the hippocampus corresponding to dentate gyrus (DG), CA1, CA2, and CA3 was done. Two independent quantifications of amyloid aggregates were performed blindly, and the same trends were observed for the two sets of values obtained. Only one quantification was kept for statistical analyses.

$A\beta_{1-42}$ Assay

For this experiment, the number of brains analyzed per group was as follows: WT CTR: $n = 4$; WT T: $n = 4$; J20 CTR: $n = 5$; and J20 T $n = 6$ (Figure 1C, Study 1). Hemi-brains were homogenized as described previously (Lafon et al. 2018). Briefly, frozen left hemispheres were homogenized in 20% wt/vol in a homogenization buffer [140 mM potassium chloride (KCl), 10 mM sodium hydrogen phosphate (Na_2HPO_4), 1.7 mM monopotassium phosphate (KH_2PO_4), and 1 mM ethylenediaminetetraacetic acid (EDTA)] containing protease inhibitors (Complete Ultra, Roche) and phosphatases inhibitors (PhosStop™, Sigma). Homogenization was performed in microbead-containing tubes on a Ribolysor apparatus (Biorad). Samples were aliquoted and immediately frozen at −80°C until use. For the $A\beta_{1-42}$ assay, 2% sodium dodecyl sulfate (SDS) was added to brain homogenates before ultracentrifugation at 196,000 × *g* (Beckman Optima TL100 centrifuge) for 30 min at 4°C. Supernatants obtained were used to quantify soluble fractions of human $A\beta_{1-42}$ peptides with an enzyme-linked immunosorbent assay kit (Invitrogen). Results were normalized according to their protein concentration determined by the bicinchoninic acid (BCA) method protein assay (Pierce Biotechnology).

Detection by Immunohistochemistry of Cypro, Mepa, and Pyri on Brain Tissue Sections of J20 Mice Treated with a Cocktail of Fungicides for 9 Months

For this experiment, the number of brains analyzed per group was as follows: J20 CTR: $n = 7$ and J20 T: $n = 8$ (Figure 1C, Study 1). Three to six floating brain tissue sections per mouse were rinsed, mounted on Superfrost® Plus glass slides, and then dried overnight at RT. Prior to amyloid labeling, brain sections were incubated for 10 min with a 70% formic acid solution for antigen retrieval. Sections were then incubated 1 h at RT with a blocking solution (3% goat serum, 0.3% Triton X100 in PBS) and incubated overnight at 4°C with the 6E10-Alexa488 antibody (1:1,000). Then, sections were washed and incubated with the antibodies anti-cypro, anti-mepa, or anti-pyri, alone or in cocktail, for 2 h at RT, followed by a 2-h incubation with a goat anti-mouse Cy3 antibody (1:1,000). Sections were counterstained with DAPI (1:50,000 in PBS). Control tissue sections were incubated either with PBS or the secondary antibody Cy3 alone. Images were taken with a Leica DM2500 microscope (magnification ×20).

Immunohistochemistry and Quantifications

For this experiment, the number of brains analyzed per group was as follows: WT CTR: $n = 3$; WT T: $n = 3$; J20 CTR: $n = 4$; and J20 T $n = 4$ (Figure 1C, Study 2). Neuroinflammation was assessed with a mouse anti-GFAP antibody (1:1,000; Sigma-Aldrich) for astrogliosis or with a rabbit polyclonal anti-IBA1 antibody (1:750; Wako Chemicals) for microgliosis. Neurons were analyzed with a mouse anti-NeuN antibody (1:500, clone A60; Merck-Millipore). Briefly, brain tissue sections were blocked 1 h at RT and incubated with one of the primary antibodies overnight at 4°C. Then, sections were washed and incubated with secondary antibodies, a goat anti-mouse Cy3 (1:1,000) or a goat anti-rabbit Alexa488 (1:1,000) for 2 h at RT. Nuclei were stained with DAPI (1:50,000). Images were taken with a Leica DM2500 microscope (magnifications: ×20 and ×40) and quantifications were performed with Fiji software in the DG, CA1, CA2, and CA3.

Astrogliosis was evaluated by quantifying the number of astrocytes (proliferation), the intensity of the labeling (expression of GFAP) and the area labeled (hypertrophy). To avoid saturation of the GFAP signal, all hippocampi were previously visualized on the microscope using the LAS software (version. 4.10; Leica Microsystems) tool named show under- and over-exposure in the viewer in order to find the best image acquisition settings (intensity and gain) without overexposure of the labeling. The same acquisition settings were kept for all the conditions and hippocampi studied (intensity: 355.9 ms; gain: 10.1×; and γ: 1.53). The intensity and the area of the labeling were measured on 8-bit images using the threshold tool of the FIJI software. The same threshold parameters were used for all images.

The total number of microglial cells and the activated subset were quantified as described previously by Mansuy et al. (2018). To decipher the subset of activated microglial cells from the quiescent ones, quantifications were performed based on their morphological differences. The ramified IBA1-positive cells with small soma and long processes were considered to be quiescent cells, whereas IBA1-positive cells with enlarged soma, short processes, and decreased branching were considered to be activated microglial cells (ameboid).

The number of NeuN-positive neurons was quantified in the four different regions of the hippocampus, presented above, and was normalized by the surface area of the granular cell layers analyzed. All the results are presented as mean ± SEM.

Interleukins and Cytokines Assays by HTRF®

For this experiment, the number of brains analyzed per group was as follows: WT CTR: $n = 3$; WT T: $n = 3$; J20 CTR: $n = 4$; and J20 T $n = 4$ (Figure 1C, Study 2). Two percent SDS was added to brain homogenates prepared as described above, which were then centrifuged at 14,000 rpm, for 20 min at 4°C. IL1β,

IL6, and tumor necrosis factor α (TNFα) levels were determined using HTRF® assay kits (Cisbio). According to the manufacturer's protocol, 16 µL of supernatant were mixed with 2 µL of donor antibody coupled to Eu^{3+}-cryptate and 2 µL of acceptor antibody coupled to d2, both antibodies recognizing IL1β, IL6, or TNFα. The mix was incubated 1 h (IL6 and TNFα) or overnight (IL1β) at 25°C. Standard curves of each kit were made in the same homogenization buffer used for samples, containing SDS. The FRET signal was measured using the d2 acceptor emission (665 nm) and the Eu^{3+}-cryptate donor emission (620 nm) with a 100-µs lag time and a 400-µs integration time after excitation at 337 nm on a Spark® 20 M (Tecan). The HTRF® ratio (signal 665 nm/620 nm × 10^4) was calculated to normalize the different wells. Results were then normalized according to their protein concentration as determined by BCA.

Dynamics of Aggregation in Vivo*: Longitudinal Study Using Two-Photon Microscopy*

In a third independent cohort, we performed a longitudinal study of appearance of aggregates as described by Arango-Lievano et al. (2016) and Giannoni et al. (2016) on J20 mice treated with fungicides (T: $n = 5$) or with an equivalent volume of DMSO (CTR: $n = 3$) (Figure 1D, Study 3). Briefly, mice were injected ip with 10 mg/kg of Methoxy-XO4 (Tocris Bioscience) to stain amyloid aggregates, 48 h before imaging. Animals were anesthetized (16% ketamine, 4% xylazine in NaCl 0.9%) and injected in the retro-orbital sinus with 100 mg/kg of dextran–fluorescein isothiocyanate (dextran-FITC) (70 kDa) on the day of imaging to stain blood vessels. The longitudinal study was performed at 3, 6, and 9 months of treatment on the same animals. Images were acquired through a thinned skull window on a head restrained mouse using a Zeiss LSM7 two-photon microscope with a 20× objective. A first stack of images was taken with a 0.7× numerical zoom (size of image 500 µm × 500 µm) in order to be able to locate the same brain area at each time point. Then, this selected region was divided into four equal areas and a stack of images was acquired with a 2× numerical zoom (200 µm × 200 µm) with a 1-µm step. The number of aggregates was quantified using Fiji software on an equal number of images. Imaris software (version 8.0; Bitplane) was used for a three-dimensional (3D) reconstruction of the stacks, and the volume of aggregates was quantified and normalized by the total volume of the stack.

Immunoblotting

For this experiment, the number of brains analyzed per group was as follows: WT CTR: $n = 3$; WT T: $n = 3$; J20 CTR: $n = 4$; and J20 T: $n = 4$ (Figure 1C, Study 2). Immunoblotting was performed as described previously (Lafon et al. 2018). Briefly, brain homogenates to which 2% SDS had been added were centrifuged at 14,000 rpm, 20 min at 4°C, to remove membrane debris. Protein concentration was measured on supernatants by BCA protein assay, and samples were all normalized to the same concentration and diluted (1:1) in 2× loading buffer [0.1 M dithiothreitol (DTT), 3% SDS, 20% glycerol, 0.4 M Tris-HCl at pH 7.4, bromophenol blue]. Samples were boiled 10 min at 90°C before loading on a 4–15% SDS–polyacrylamide gel electrophoresis (SDS-PAGE) gradient precast gel (Biorad). After protein transfer, PVDF membranes were blocked in 5% nonfat milk solution and were incubated overnight at 4°C with one of the following primary antibodies: anti-β-amyloid 1-16 antibody (6E10 clone, 1:1,000; Biolegend), anti-APP A4 polyclonal antibody (22C11 clone, 1:1,000; Merck-Millipore), anti-BACE1 polyclonal antibody (1:500; Cell Signaling Technology), anti-IDE polyclonal antibody (1:1,000; Abcam), anti-LRP1 polyclonal antibody (1:30,000; Abcam), or an anti-NEP polyclonal antibody (1:2,000; Merck-Millipore). Then, membranes were incubated for 2 h at RT with the corresponding secondary antibodies: peroxidase-conjugated anti-mouse antibody (1:10,000; Jackson ImmunoResearch) or anti-rabbit (1:5,000; Jackson ImmunoResearch). Protein loading controls were performed with a mouse anti-β-actin antibody (1:1,000; Sigma-Aldrich). Membranes were revealed with a ChemiDoc™ MP Imager (Biorad) using the signal accumulation mode, and signals were quantified on the Image Lab software (version 6.0.1; Biorad).

mRNA Extraction and Real-Time qPCR

For this experiment, the number of brains analyzed per group was as follows: WT CTR: $n = 3$; WT T: $n = 3$; J20 CTR: $n = 4$; and J20 T: $n = 4$ (Figure 1C, Study 2). Total mRNA was extracted from brain homogenates with the Nucleospin RNA extraction kit (Macherey Nagel), according to the manufacturer's instructions. RNA quality and concentrations were measured in a NanoDrop™ 8,000 spectrophotometer (Thermo Scientific). mRNA was reverse-transcribed with a high-capacity circular-DNA reverse transcription kit (Applied Biosystems, ThermoFisher Scientific) and amplified by real-time PCR (RT PCR) with a Light Cycler detection system (Roche) according to the manufacturer's instructions. RT-qPCR was performed in collaboration with the qPCR Haut Débit (qPHD) platform (University of Montpellier, France) following the Minimum Information for Publication of Quantitative Real-Time PCR Experiments (MIQE) guidelines (Bustin et al. 2009), and β-*actin* was used as a reference gene. The ΔC_t value of the reference and target genes was quantified as described previously (Nasri et al. 2016). For each target gene tested, experiments were performed three times independently and in triplicate. Primers (Eurogentec) used for RT-qPCR are listed in Table S1.

Statistical Analyses

All data were initially analyzed on GraphPad Prism software (version 5.0; GraphPad) using Shapiro-Wilk's normality test. When data sets were normally distributed ($p > 0.05$), statistical analyses were performed using parametric tests: multiple *t*-test (Holm-Sidak's correction), the student's *t*-test, the linear correlations, or the two-way analysis of variance (ANOVA; Holm-Sidak's post hoc analysis). However, when data sets were not normally distributed ($p < 0.05$) statistical analyses were performed using a nonparametric test: Mann-Whitney *U*-test. A probability of 0.05 has been defined as a significant difference for all statistical analyses.

Results

Ex Vivo *Binding of Cypro, Mepa, and Pyri to Amyloid Plaques and Their Effects on the Kinetics of $A\beta_{1-42}$ Fibril Formation* in Vitro

We first evaluated whether cypro, mepa, and pyri could bind to amyloid plaques *ex vivo*. Brain tissue sections from 10-month-old J20 mice were incubated with 2 mM of these fungicides, either alone or in cocktail, for 1.5 h at RT. Primary antibodies against cypro (Esteve-Turrillas et al. 2012), mepa (Esteve-Turrillas et al. 2013), and pyri (Mercader et al. 2012) were used to detect them (Figure 2A, column 3). Amyloid aggregates were revealed using a 6E10 antibody conjugated to Alexa488 (Figure 2A, column 2). Remarkably, the merge column showed that fungicides, either incubated alone or in cocktail, bound to amyloid plaques *ex vivo* (Figure 2A 2–6). There was no nonspecific staining in controls when using an equivalent volume of DMSO (1%) corresponding to the cocktail condition (Figure 2A 1). Given that these antibodies

were used for the first time for histological studies, further controls are presented in Figure S1.

Because anilinopyrimidines bound to amyloid plaques *ex vivo*, we wondered whether they could modify the kinetic profile of $A\beta_{1-42}$ fibrils *in vitro*. $A\beta_{1-42}$ monomers were obtained by size exclusion chromatography to exclude oligomeric species as described by Serra-Batiste et al. (2016). For the kinetics of amyloid fibril formation, $A\beta_{1-42}$ monomers were mixed with the three anilinopyrimidines at a molar ratio of 1:1 (Aβ:fungicides) (Figure 2B, triangles) or of 1:15 (Figure 2C, squares). Control conditions were performed with an equivalent volume of DMSO (1%; Figure 2B, crosses, and 2C, circles). Tubes were incubated at 25°C and fibril formation was monitored by ThT, once a day. We found that the presence of fungicides dramatically modified the kinetic profile by accelerating the formation of $A\beta_{1-42}$ fibrils at both ratios. These processes were shifted through a substantial decrease of the lag phase and an increased level of ThT fluorescence at the plateau phase compared with control conditions (Figure 2B,C).

Body Weight, Water Consumption, and Pesticide Ingestion of Mice Treated with the Cocktail of Fungicides or with DMSO

Our aim was to determine the impact of those three fungicides on different markers of Alzheimer's disease *in vivo*. First, we assessed the impact of the cocktail of the fungicides on different physical parameters. From the weaning of mice until the end of the treatment 9 months later (35 weeks), neither WT nor J20 mice exhibited a modification of body weight gain upon treatment for either females (see Figure S2A) or males (see Figure S2B). Water consumption was estimated per mouse and per week for each group. The treatment with fungicides did not modify the drinking behavior for either females (see Figure S2C) or males (see Figure S2D) compared with their respective DMSO-treated mice (CTR). However, when comparing WT and J20 mice treated with the cocktail of fungicides, we noticed that transgenic mice drank more water than their WT littermates, for both females (see Figure S3A, 23.46 ± 0.38 mL/week for WT T vs. 27.88 ± 0.90 for J20 T, $p < 0.001$) and males (see Figure S3B, 25.18 ± 0.44 mL/week for WT T vs. 34.64 ± 0.60 for J20 T, $p < 0.001$). Estimation of fungicides ingestion per mouse and per week revealed that J20 female mice treated with the cocktail of fungicides ingested a significantly higher level of pesticides than their WT littermates (see Figure S3C, 2.418 ± 0.034 ng of fungicides for WT T vs. 2.788 ± 0.09 for J20 T, $p = 0.0023$). A similar difference in fungicide ingestion was observed between WT and J20 males (see Figure S3D, 2.518 ± 0.044 ng for WT T vs. 3.387 ± 0.061 for J20 T, $p < 0.001$).

In Vivo *Effect of Fungicides on Soluble and Aggregated $A\beta_{1-42}$ in J20 Mice*

WT and J20 mice were treated with 0.1 μg/L of cypro, mepa, and pyri administered as a cocktail through drinking water (referred to as T) (Figure 1, Study 1). Control groups of WT and J20 mice were treated with an equivalent volume of DMSO (3×10^{-5} %, referred to as CTR) (Figure 1, Study 1). Treatment started after weaning of mice and lasted 9 months, so mice were sacrificed at 10 months of age. The impact of the cocktail of fungicides on amyloid aggregates was carried out by histological analyses using ThT staining (Figure 3). First, we quantified the number and the size of aggregates in the hippocampus and the cortex, taking into account sex differences. Results showed no differences in the number or size of amyloid plaques between males and females after 9 months of treatment (see Figure S4; $p > 0.05$); therefore, results were pooled for statistical analyses. As expected, WT mice treated either with DMSO (CTR) or with the cocktail of fungicides (T) did not exhibit ThT-positive aggregates at this stage [Figure 3A (left panel) and 3B–E]. Treatment of J20 mice with the cocktail of fungicides (J20 T) for 9 months significantly increased the number of ThT-positive aggregates [Figure 3A (right panel)] by 26% and 53% in the hippocampus and the cortex, respectively (Figure 3B,D; hippocampus: 421 ± 29.4 aggregates/cm^2 for J20 CTR vs. 530 ± 23.7 for J20 T, $p = 0.003$ and cortex: 173.9 ± 14.6 for J20 CTR vs. 266.5 ± 23.1 for J20 T, $p < 0.001$). The treatment with fungicides also significantly modified the surface area of ThT-positive plaques by 42% in the hippocampus (Figure 3C; 0.279 ± 0.026 A.U. for J20 CTR vs. 0.397 ± 0.025 for J20 T, $p = 0.002$) as well as by 80% in the cortex (Figure 3E; 0.108 ± 0.01 for J20 CTR vs. 0.194 ± 0.018 for J20 T, $p < 0.001$). Distribution of aggregates in the different areas of the hippocampus (DG, CA1, CA2, and CA3) revealed the higher number of plaques in J20 T mice to be essentially located in the CA1 region (Figure 3F; 108.1 ± 12.1 aggregates/cm^2 for J20 CTR vs. 172.7 ± 26.8 for J20 T, $p = 0.04$). The same effect in the CA1 area was noticed for the surface area of ThT-positive aggregates (Figure 3G; 0.075 ± 0.007 A.U. for J20 CTR vs. 0.135 ± 0.019 for J20 T, $p = 0.03$). Soluble human $A\beta_{1-42}$ levels were assayed in supernatants from ultracentrifuged brain homogenates. J20 treated mice exhibited almost three times more soluble $A\beta_{1-42}$ compared with the control DMSO-treated mice (Figure 3H; 0.465 ± 0.212 pg/mg of proteins for J20 CTR vs. 1.323 ± 0.140 for J20 T, $p = 0.02$).

Attempts to Detect Cypro, Mepa, and Pyri in Situ *in J20 Mice Brain Tissue Sections Treated for 9 Months with a Cocktail of Fungicides*

We believed that after a long-term exposure of fungicide those compounds could potentially accumulate in brains, especially in amyloid aggregates, based on our *ex vivo* and *in vitro* binding results. To evaluate this, brain tissue sections from J20 mice treated (J20 T, $n = 7$) or not (J20 CTR, $n = 8$) with 0.1 μg/L of fungicides during 9 months were analyzed (Figure 1C, Study 1). Tissues were first labeled with the 6E10-Alexa488 antibody to detect amyloid aggregates, and then, anti-fungicide antibodies (anti-cypro, -mepa, -pyri) were used to reveal their potential accumulation in Aβ plaques. As a control for the specificity of the fungicide labeling, DMSO-treated J20 brain tissue sections were used. As expected, no labeling was detected in the red channel (see Figure S5A-F, column 3). Regarding brain tissue sections from J20 mice treated with the cocktail of fungicides, antibodies raised against cypro, mepa, and pyri were not able to detect the presence of the fungicides in the amyloid aggregates *in situ* (see Figure S6A-F).

Effect of the Cocktail Treatment on Neuroinflammation Processes

Astrogliosis analyses. To determine the impact of the chronic pesticide exposure on the activation of astrocytes, we performed an immunohistochemistry evaluation on brain tissue sections with an anti-GFAP antibody and analyzed the different areas of the hippocampus (DG, CA1, CA2, and CA3) (Figure 4A). We quantified the intensity of the labeling reflecting GFAP expression and the surface area of the labeling to measure the hypertrophy of astrocytes (Figure 4B–E). The number of GFAP-positive cells is presented in Figure S7. Regarding J20 mice, treatment with fungicides significantly up-regulated GFAP expression in the CA1 area, reflecting an astrogliosis [Figure 4C (left panel); $1{,}749 \pm 285.8$ A.U. for J20 CTR vs. $3{,}456 \pm 478.1$ for J20 T, $p = 0.030$]. A tendency of up-regulation of GFAP was observed in the DG although it was not statistically significant [Figure 4B (left panel)]. In addition, in J20 T mice, both DG and CA1 exhibited

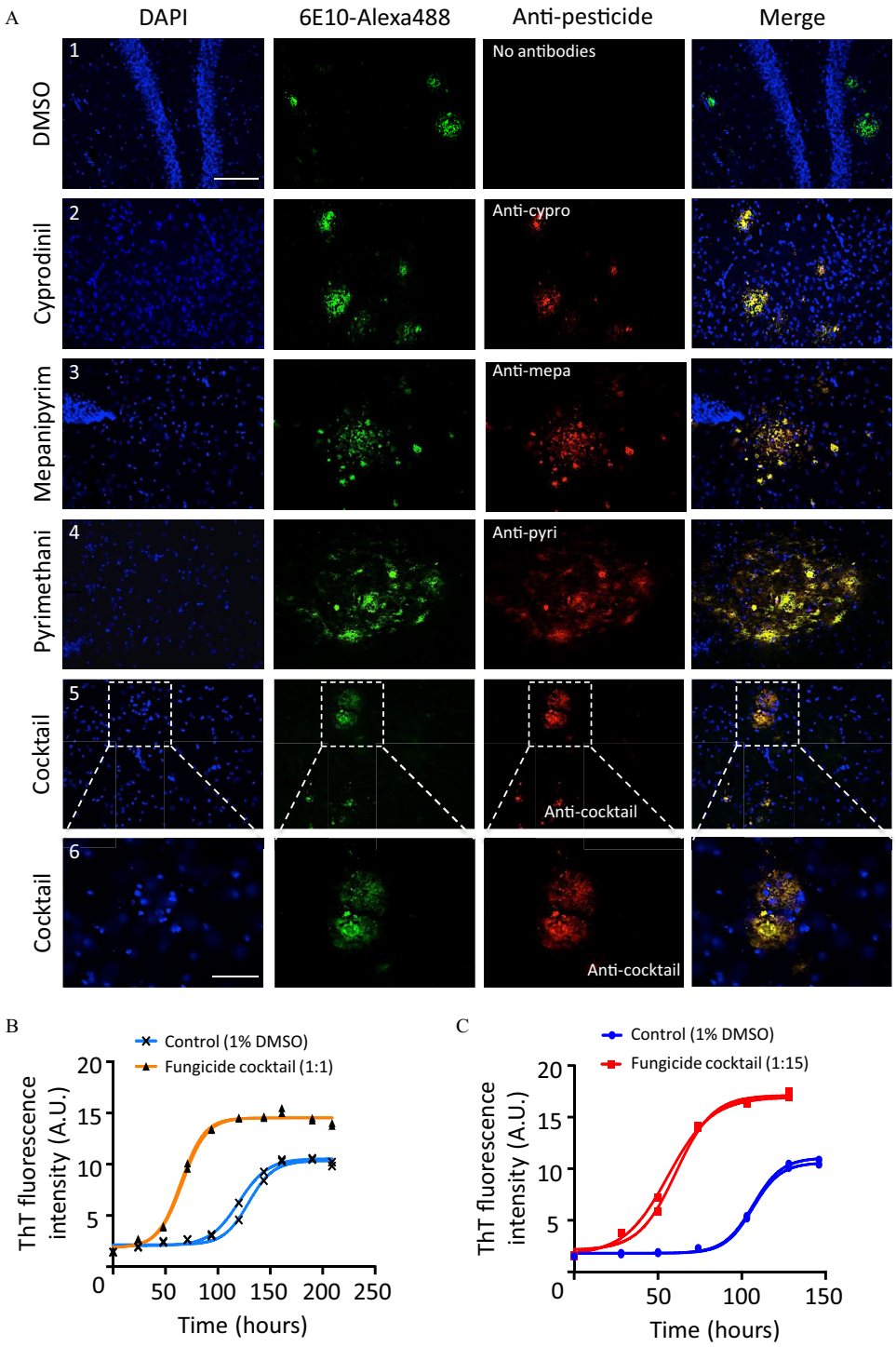

Figure 2. (A) *Ex vivo* co-localization of cyprodinil, mepanipyrim, and pyrimethanil with Aβ aggregates on J20 brain tissue sections and (B,C) kinetics of $A\beta_{1-42}$ fibril formation with a cocktail of the three fungicides. (A) Brain tissue sections from 10-month-old J20 mice were incubated for 90 min at room temperature with 2 mM of either cyprodinil (A2), mepanipyrim (A3), pyrimethanil (A4), a cocktail of the three fungicides (A5-6), or an equivalent volume of DMSO (1%) as a control (A1). Sections were labeled with an anti-human β-amyloid 6E10-Alexa488 and anti-cypro, anti-mepa, or anti-pyri antibodies. Aβ aggregates are seen in the green channel (column 2) and the different fungicides in the red channel (column 3). No red fluorescence was observed in the control condition (A1). The Merge column showed the co-localization of the fungicides with amyloid aggregates, and higher enlargements are presented in the panel A6 for the cocktail. For each condition, three to six sections were analyzed and independent experiments were performed at least three to six times. Images selected are representative of the labeling observed in different regions of the hippocampus (A1,3: dentate gyrus; A4: near dentate gyrus; A2,5–6: near CA1 area). Scale bars: 100 μM (A1–5: magnification ×20) and 50 μm (A6: magnification ×40). (B) Effect of a cocktail of fungicides on the kinetics of Aβ fibril formation. Human $A\beta_{1-42}$ monomers (30 μM) were incubated at a molar ratio 1:1 with a cocktail of cypro, mepa, and pyri (30 μM each) (triangles) or with an equivalent volume of DMSO (1%) (crosses). ThT fluorescence intensity was measured once a day (A.U., arbitrary units). For each condition, independent experiments were performed in duplicate. The different values obtained were plotted following a sigmoidal fit and representative curves of duplicates were presented. (C) Effect of a cocktail of fungicides on the kinetics of Aβ fibrils formation with a molar ratio 1:15 (30 μM Aβ: 750 μM of each fungicide) (squares). Control conditions were performed with an equivalent volume of DMSO (1%) (circles). ThT fluorescence intensity was measured once a day (in A.U.). For each condition, independent experiments were performed in duplicate. The different values obtained were plotted following a sigmoidal fit and representative curves of duplicates were presented. Note: DAPI, 2-(4-amidinophenyl)-1*H*-indole-6-carboxamidine; DMSO, dimethyl sulfoxide; ThT, thioflavin T.

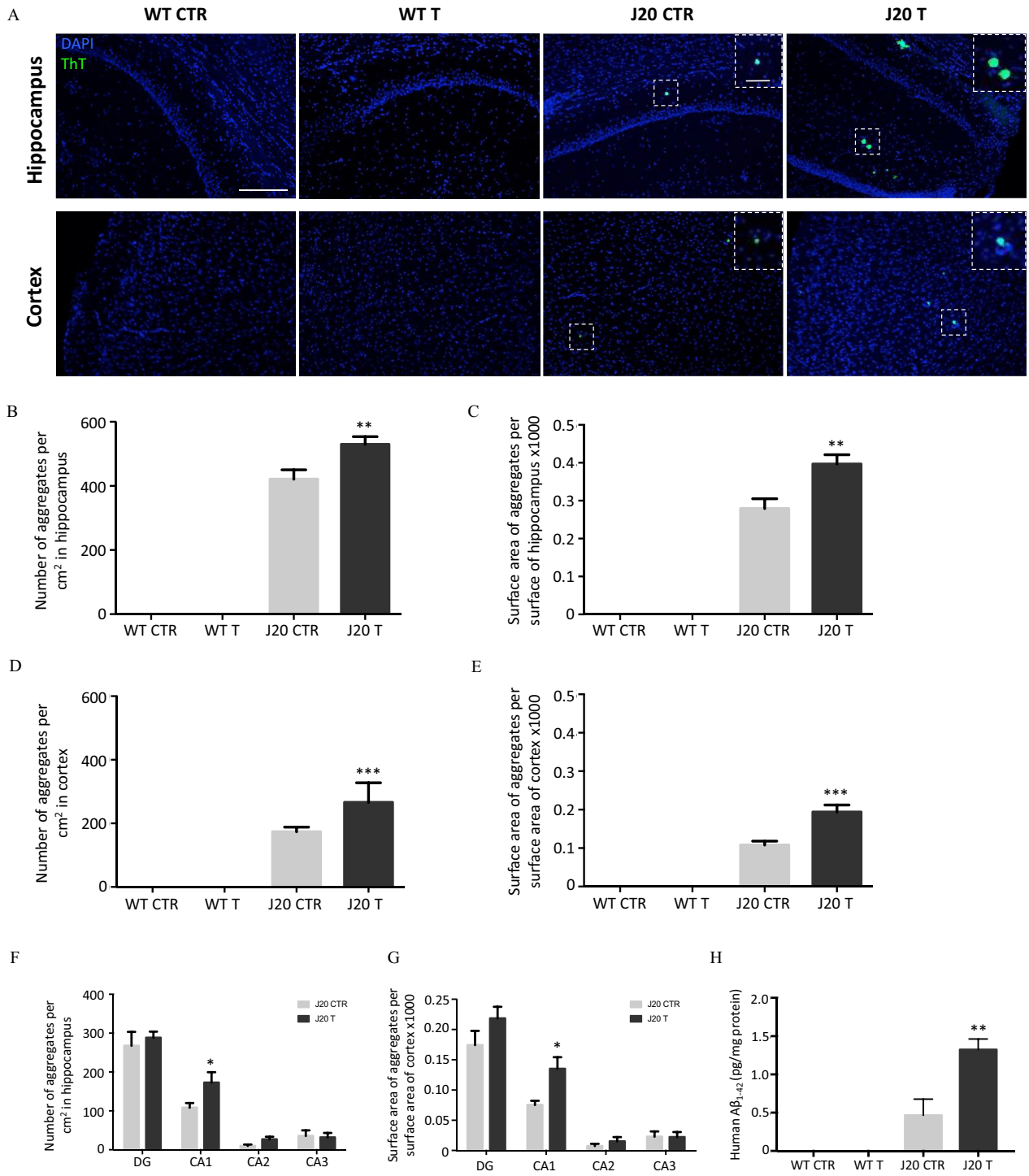

Figure 3. (A) Thioflavin T (ThT) staining of brain sections of WT and J20 mice treated with the cocktail of fungicides or with DMSO for 9 months, (B,C,F,G) quantification of aggregates in the hippocampus, (D,E) in the cortex and (H) human soluble $A\beta_{1-42}$ assay. (A) Representative images of amyloid plaques stained with ThT (in green) in the hippocampus and in the cortex of WT and J20 mice treated with the cocktail of fungicides (0.1 μg/L each) (T) or with an equivalent volume of DMSO (3×10^{-5} %) (CTR) (Scale bar: 100 μm, magnification ×20). Inserts are enlargements of representative aggregates (scale bar: 50 μm, magnification ×40). (B–E) Quantifications of the number (B,D) and the surface area (C,E) of ThT-positive aggregates in WT and J20 mice (T and CTR), normalized by the total surface area of hippocampus or cortex analyzed. Aggregates were quantified using Fiji software. The number of aggregates are expressed as mean ± SEM/cm^2 and their surface area as mean ± SEM × 1,000 (without units). Statistical differences were calculated using a two-way ANOVA followed by a Holm-Sidak's post hoc analysis. (F,G) The number (F) and surface area (G) of aggregates in the hippocampus were quantified in the different areas: dentate gyrus (DG), CA1, CA2, and CA3 for the J20 mice (T and CTR). Values are expressed as mean ± SEM and statistical differences were calculated using a multiple *t*-test followed by a Holm-Sidak's post hoc analysis. For all histological analyses, 8–10 brain tissue sections per animal were used (A–G). (H) Soluble forms of human $A\beta_{1-42}$ in WT and J20 mice treated with the fungicides (T) or with DMSO (CTR) were quantified on supernatants of ultracentrifuged brain homogenates by ELISA. Results were normalized by protein concentration and are expressed as mean ± SEM (pg of $A\beta_{1-42}$/mg of proteins). Statistical differences were obtained using a two-way ANOVA followed by a Holm-Sidak's post hoc analysis. For all statistical tests a probability of 0.05 was defined as a significant difference ($^{*}p < 0.05$, $^{**}p < 0.01$, $^{***}p < 0.001$). $n = 4$–8 mice per group issued from Study 1. Note: ANOVA, analysis of variance; CTR, control; DAPI, 2-(4-amidinophenyl)-1*H*-indole-6-carboxamidine; DMSO, dimethyl sulfoxide; ELISA, enzyme-linked immunosorbent assay; T, treatment; WT, wild type.

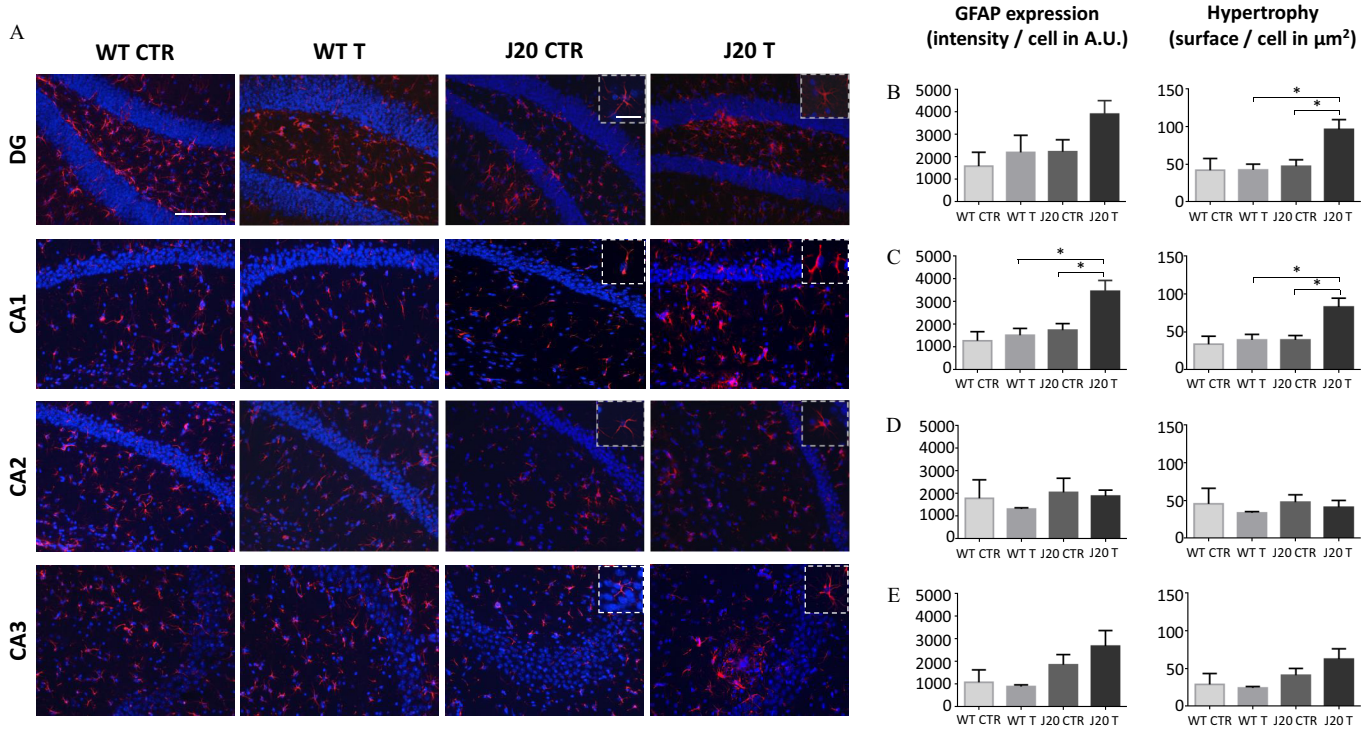

Figure 4. (A) Astrocyte labeling in the hippocampus of WT and J20 mice treated with the fungicide cocktail or with DMSO for 9 months and (B) quantification of GFAP expression and hypertrophy of astrocytes in the dentate gyrus (DG), (C) CA1, (D) CA2, and (E) CA3 areas. (A) Representative images of brain tissue sections labeled with an anti-GFAP antibody to visualize astrocytes. Brain tissue sections from WT and J20 mice, either treated with the cocktail of fungicides (0.1 µg/L each) (T) or with an equivalent volume of DMSO (3×10^{-5}%) (CTR) for 9 months were used to quantify the intensity (astrogliosis) and the surface area (hypertrophy) of the GFAP labeling. Results were normalized by the total number of cells. These parameters were quantified on 8–10 hippocampus per animal, for the DG (B), the CA1 (C), the CA2 (D), and the CA3 (E) areas. Values are expressed as mean ± SEM and a two-way ANOVA followed by a Holm-Sidak's post hoc analysis was used to evaluate statistical differences ($\alpha = 0.05$, $^{*}p < 0.05$). Scale bar: 100 µm (magnification ×20). Inserts are representative images of the astrocyte status in the different groups (scale bar: 50 µm, magnification ×40). $n = 3$–4 animals per group issued from Study 2. Note: A.U., arbitrary units; ANOVA, analysis of variance; CTR, control; DMSO, dimethyl sulfoxide; GFAP, glial fibrillary acidic protein; T, treatment; WT, wild type.

a hypertrophy of astrocytes upon treatment [Figure 4B,C (right panels)] (in DG: 47.3 ± 8.6 µm²/cell for J20 CTR vs. 96.4 ± 13.1 for J20 T mice, $p = 0.047$; in CA1: 39.4 ± 5.9 for J20 CTR vs. 82.9 ± 11.6 for J20 T, $p = 0.028$). Regarding the number of astrocytes, treatment had an impact only on WT mice in the CA2 region (see Figure S6C; 375.7 ± 99.9 astrocytes/mm² for WT CTR vs. 651.1 ± 34.1 for WT T, $p = 0.027$), but was not associated with an up-regulation of GFAP expression or a hypertrophy of astrocytes (Figure 4D).

Microgliosis analyses. To study microglial cells, we performed histological analyses using the constitutive marker, IBA1 (Figure 5A). Labeling in the hippocampus was quantified as the total number of IBA1-positive cells and the ameboid ones in the DG, CA1, CA2, and CA3 areas (Figure 5B–E). For J20 mice, the total number of microglial cells was greater upon treatment with fungicides than in mice treated with vehicle in all regions analyzed [Figure 5B–E (left panels); DG: 266.7 ± 9.9 for J20 CTR vs. 518.1 ± 47.2 for J20 T, $p < 0.001$; CA1: 148.4 ± 11.8 for J20 CTR vs. 217.9 ± 7.5 for J20 T, $p = 0.0036$; CA2: 150.7 ± 8.2 for J20 CTR vs. 268.3 ± 25.8, $p = 0.0029$ and CA3: 193.5 ± 5.3 for J20 CTR vs. 272.6 ± 23.9 for J20 T, $p = 0.014$]. The treatment also resulted in a greater number of activated microglial cells in all regions apart from CA1 (DG: 95.17 ± 11.01 activated microglia/mm² for J20 CTR vs. 178.9 ± 21.07 for J20 T, $p = 0.006$; CA2: 43.97 ± 3.3 for J20 CTR vs. 75.36 ± 8.09, $p = 0.019$; and CA3: 44.77 ± 4.34 for J20 CTR vs. 76.34 ± 6.87 for J20 T, $p = 0.006$). Analysis of microglial cells in WT mice did not reveal any difference upon treatment with the cocktail of fungicides in the hippocampus (Figure 5A–E).

Interleukins and cytokines secretion. Because brain inflammatory processes involve the secretion of pro-inflammatory interleukins and cytokines, we next measured levels of IL1β (IL1β), IL6, and TNFα in brain homogenates by HTRF® (Figure 6). Brains from J20 mice treated with fungicides exhibited a 1.6-fold higher level of IL1β (Figure 6A; 10.74 ± 1.18 pg/mg for J20 CTR vs. 17.72 ± 1.15 for J20 T, $p = 0.093$) and a nearly 3-fold higher level of IL6 (Figure 6B; 0.39 ± 0.05 pg/mg for J20 CTR vs. 1.09 ± 0.15 pg/mg for J20 T, $p = 0.0429$). However, TNFα levels were unchanged in the J20 mice treated with the cocktail of fungicides compared with J20 CTR mice (Figure 6C). There were no differences in WT mice treated with or without the fungicide cocktail (Figure 6A,C) apart from a slight nonsignificant increase in IL6 levels (Figure 6B).

Effect of the Chronic Fungicide Treatment on the Hippocampal Neuronal Loss

We wondered whether the treatment with the cocktail of fungicides could also impact hippocampal neuronal loss. To this aim, we labeled brain tissue sections with an anti-NeuN antibody to study undamaged neurons in the four different areas of the hippocampus (DG, CA1, CA2, and CA3) (Figure 7). Remarkably, in WT animals, analyses revealed that treatment with the cocktail of fungicides increased the number of neurons in the CA1 and CA3 areas (Figure 7C,E) [means ± standard error means (SEMs) and statistical analyses for WT mice are presented in Table S2]. Interestingly, J20 mice exhibited a significant decrease of the number of neurons in the CA3 region compared with DMSO-treated animals (Figure 7E, 2,386 ± 120.7 neurons/mm² of granular cell layers for J20 CTR vs. 1,978 ± 71.21 for J20 T, $p = 0.0258$) (means ± SEMs and statistical analyses for J20 mice are presented in Table S3).

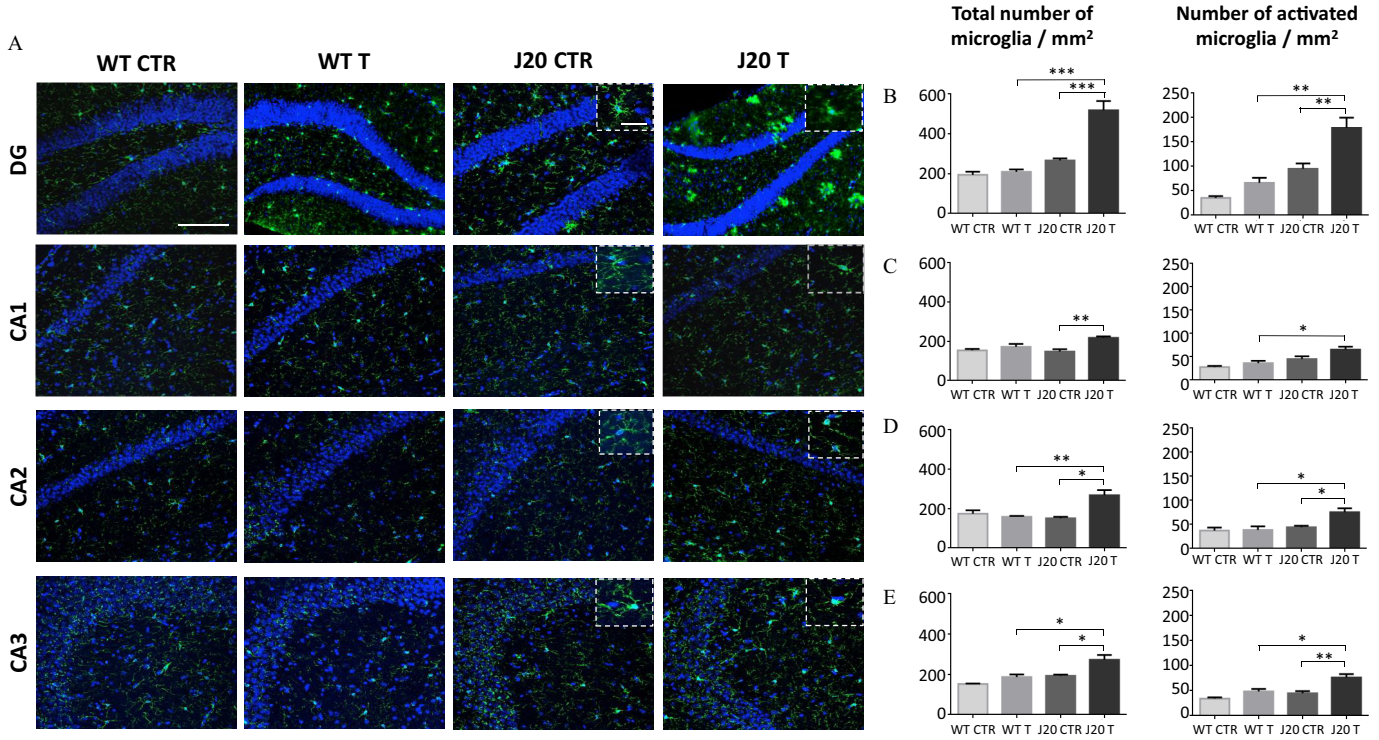

Figure 5. (A) Microglial labeling of WT and J20 mice treated with 0.1 μg/L of a cocktail of fungicides or with DMSO for 9 months and quantification of the number of total microglial cells and the activated subset in the (B) dentate gyrus (DG), (C) CA1, (D) CA2, and (E) CA3 areas. (A) Representative images of tissue sections from WT and J20 mice, labeled with an anti-IBA1 antibody, in different regions of the hippocampus. Animals were treated with a cocktail of fungicides (0.1 μg/L each) (T) or with an equivalent volume of DMSO (3×10^{-5}%) (CTR) for 9 months. The numbers of total and activated (ameboid) microglial cells per mm^2 were quantified for the DG (B), CA1 (C), CA2 (D), and CA3 (E) regions. For all immunohistochemistry analyses, 8–10 brain tissue sections per animal were used. Values are expressed as mean ± SEM and statistical differences were measured using a two-way ANOVA followed by a Holm-Sidak's post hoc analysis ($\alpha = 0.05$, $^{*}p < 0.05$, $^{**}p < 0.01$, $^{***}p < 0.001$). Scale bar: 100 μm (magnification ×20). Inserts are representative images of the microglial cells status in the different groups (scale bar: 50 μm, magnification ×40). $n = 3$–4 animals per group issued from Study 2. Note: ANOVA, analysis of variance; CTR, control; DMSO, dimethyl sulfoxide; T, treatment; WT, wild type.

Longitudinal Study of Appearance of Aggregates in the Superficial Cortex of J20 Mice Chronically Exposed to Fungicides for 9 Months

To clarify the impact of the chronic exposure to low doses of fungicides on the progression of the amyloid burden, we studied the dynamics of aggregation *in vivo* using a longitudinal approach by two-photon microscopy. Because the J20 mouse model is also known for its cerebral amyloid angiopathy (CAA) phenotype (Kimbrough et al. 2015), we took advantage of this characteristic to monitor amyloid plaque formation on the superficial cortex over time on the same animals. In this study (Figure 1D), J20 mice treated with the cocktail of fungicides ($n = 5$) or with DMSO ($n = 3$) underwent three imaging sessions at 3, 6, and 9 months of treatment (Figures 8 and 9). Mice were injected at each time point with Methoxy-XO4, an amyloid dye (in blue but artificially colored in red) and with dextran-FITC to stain blood vessels (in green). As expected, no Methoxy-XO4-positive aggregates were detected at 3 months on the superficial cortex in both groups, given that at this age no vascular aggregates were detected (Kimbrough et al. 2015) (Figure 8A,B). In J20 CTR mice, we observed an accumulation of Aβ peptides both around blood vessels (arrows) and in the parenchyma (circles) at 6 and 9 months (Figure 8A). Strikingly, J20 mice treated with the cocktail of fungicides exhibited an enhanced perivascular aggregation (arrows) at 9

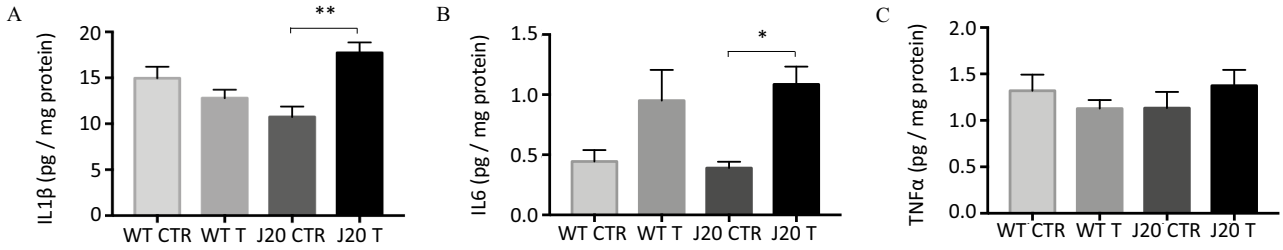

Figure 6. (A) IL1β, (B) IL6, and (C) TNFα levels in brain homogenates from WT and J20 mice treated with fungicides or with DMSO for 9 months. (A) IL1β, (B) IL6, and (C) TNFα levels were measured in brain homogenates of WT and J20 mice treated with the cocktail of fungicides (0.1 μg/L each) (T) or with 3×10^{-5} % of DMSO (CTR) for 9 months. Interleukin and cytokine levels were assayed using HTRF® kits and results were normalized by their protein concentration (BCA). Three to four different brains were analyzed in triplicate for each group issued from Study 2. Results are presented as mean ± SEM (pg/mg of proteins) and statistical differences were calculated using a two-way ANOVA followed by a Holm-Sidak's post hoc analysis ($\alpha = 0.05$, $^{*}p < 0.05$, $^{**}p < 0.01$). Note: ANOVA, analysis of variance; CTR, control; DMSO, dimethyl sulfoxide; HTRF®, homogeneous time resolved fluorescence; IL, interleukin; T, treatment; TNFα, tumor necrosis factor α; WT, wild type.

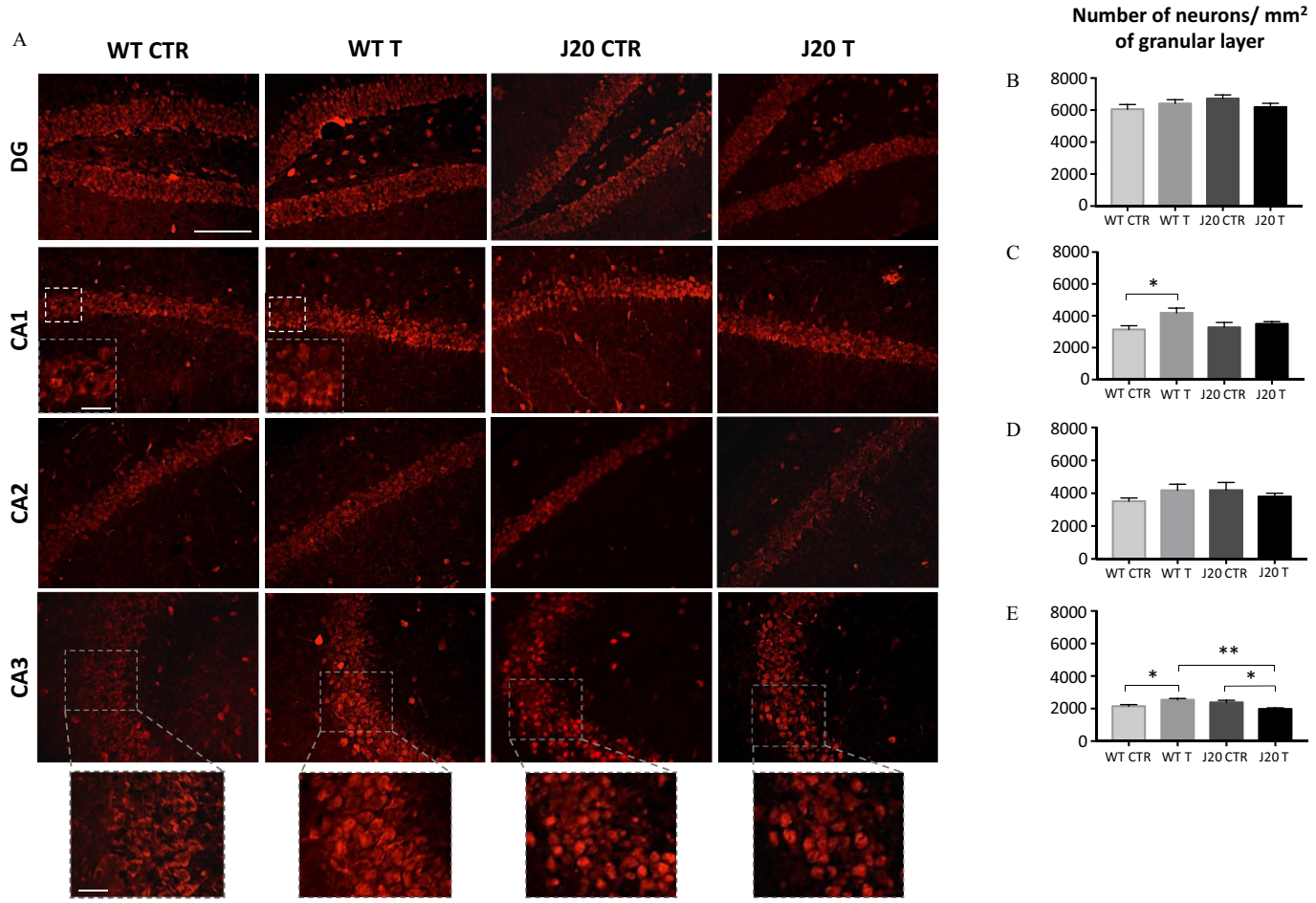

Figure 7. (A) NeuN labeling of brain tissue sections from WT and J20 mice treated with fungicides or with DMSO for 9 months and quantification of the number of neurons in the granular cell layers of the (B) dentate gyrus (DG), (C) CA1, (D) CA2, and (E) CA3 areas. (A) Representative images of hippocampal neurons labeled with an anti-NeuN antibody. Brain sections from WT and J20 mice, treated with the cocktail of fungicides (0.1 μg/L each) (T) or with an equivalent volume of DMSO (3×10^{-5} %) (CTR) during 9 months, were used for the analyses. The number of hippocampal neurons was quantified for the DG (B), CA1 (C), CA2 (D), and CA3 (E) areas and was normalized by the surface area of the granular cell layers analyzed (mm^2). Values are expressed as mean ± SEM (neurons/mm^2 of granular cell layers) and statistical differences were calculated using a two-way ANOVA followed by a Holm-Sidak's post hoc analysis with a probability of 0.05 defined as a significant difference ($^{*}p < 0.05$, $^{**}p < 0.01$). Scale bar: 100 μm (magnification ×20). Inserts are presented only when results were statistically significant and are representative images of the granular cell layers (scale bar: 50 μm, magnification ×40). $n = 3$–4 mice per group issued from Study 2. Note: ANOVA, analysis of variance; CTR, control; DMSO, dimethyl sulfoxide; NeuN, neuronal nuclei; T, treatment; WT, wild type.

months compared with their control littermates treated with DMSO (Figure 8B). We quantified the total number of aggregates as well as their distribution in the parenchyma and around blood vessels. Analyses revealed that the number of parenchymal aggregates were not impacted by the cocktail of fungicides (Figure 8D), whereas vascular aggregates were about three times higher in J20 T mice compared with J20 CTR at 9 months posttreatment (Figure 8E; 63.67 ± 12.91 for J20 CTR vs. 183.4 ± 52.66 for J20 T, $p = 0.031$). When counting the number of aggregates, we could see the fusion of some plaques between 6 and 9 months in J20 T mice, as shown by arrowheads in Figure 8B, leading to an under-quantification of their number. To overcome this bias, we performed a 3D reconstruction using Imaris software (version 8.0; Bitplane) on the stacks of images acquired at 3, 6, and 9 months of treatment to quantify the volume of aggregates (Figure 9A). In these 3D images, we found the main characteristic of CAA, which is the presence of vascular aggregates on leptomeningeal and penetrating vessels surrounded by some parenchymal aggregates (Figure 9B). We performed a quantification of the total volume of aggregates as well as the distribution between the parenchymal and vascular ones, normalized by the total volume of the stacks. Analyses showed a significant 3-fold increase of the total volume of aggregates at 9 months of treatment (Figure 9C; 60.1 ± 4.68 A.U. for J20 CTR vs. 173.9 ± 49.51 for J20 T, $p = 0.028$), mainly due to an 18-fold increase of the volume of the vascular aggregates (Figure 9E; 6.86 ± 1.15 A.U. for J20 CTR vs. 125.6 ± 60.06 for J20 T, $p = 0.023$). During this experiment, vascular aggregates were all found to be located on the blood vessel walls, except for one aggregate that was found inside a blood vessel (see Figure S8). We then performed a linear correlation between the volume of vascular and parenchymal aggregates using all the data collected at 3, 6, and 9 months posttreatment. For each mouse, three values were presented in the graph, with a total of 24 points for eight different animals (at 3 months posttreatment, all the values were null because no amyloid plaques were detected at this stage). While comparing the correlation obtained for the J20 CTR mice [Figure 9F (circles); $y = 0.127x - 0.314$, Pearson's correlation coefficient $(r) = 0.915$, $p < 0.001$] with the correlation of the J20 mice exposed to the cocktail of fungicides, we noticed the presence of two subpopulations in the J20 T group. These two subpopulations were called low responders and high responders to the fungicide treatment. We can clearly see that the correlation of the low responders group was almost similar to the one of the J20 CTR group [Figure 9F (triangles); $y = 0.158x + 0.741$, $r = 0.863$, $p = 0.0013$]. By contrast, the high responders exhibited a modified slope of the line to the benefit

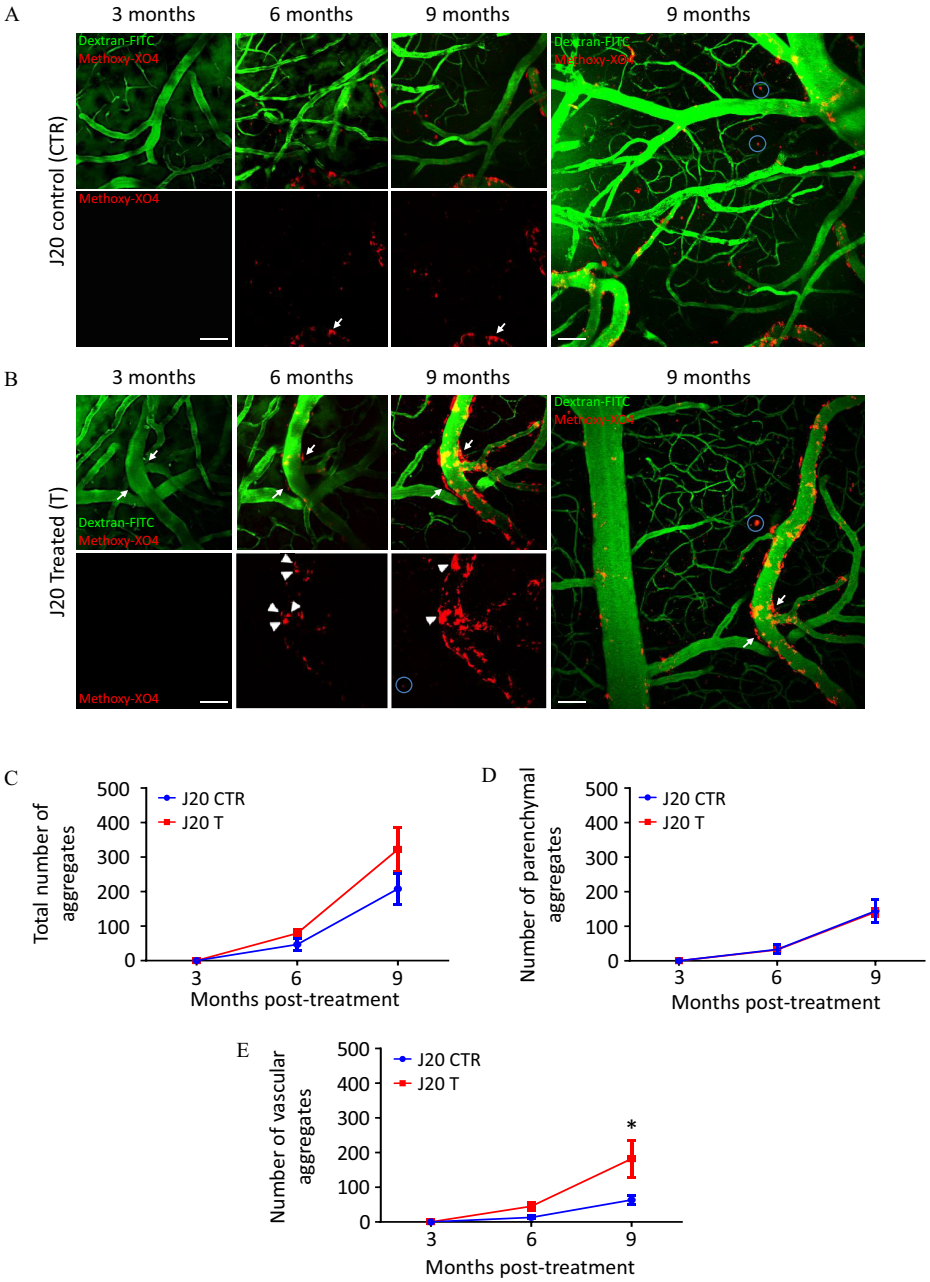

Figure 8. *In vivo* dynamics of amyloid plaque formation at 3, 6, and 9 months in the superficial cortex of J20 mice treated with (A) DMSO or (B) fungicides, and quantification of (C) total, (D) parenchymal, and (E) vascular number of aggregates. (A) Representative images taken at 3, 6, and 9 months with a two-photon microscope on the same superficial cortex area of J20 mouse treated with 3×10^{-5} % of DMSO (CTR). Mice were injected with Methoxy-XO4 (artificially colored in red) to stain amyloid aggregates, and dextran-FITC (green) to stain blood vessels. Arrows showed the progression of vascular aggregates and circles illustrated parenchymal aggregates. (B) two-photon representative images taken at 3, 6, and 9 months of the same brain area of a J20 mice treated with fungicides (0.1 µg/L each) (T). Arrows and circles showed vascular and parenchymal aggregates respectively, whereas arrowheads indicated fusion of vascular aggregates overtime. Quantification of the (C) total, (D) parenchymal, and (E) vascular number of aggregates was performed using Fiji software. Values are presented as mean ± SEM and a two-way ANOVA followed by a Holm-Sidak's post hoc analysis was used for the statistical analyses ($\alpha = 0.05$, $^{*}p < 0.05$). Scale bars: 50 µm. $n = 3$–5 animals per group issued from Study 3. Note: ANOVA, analysis of variance; DMSO, dimethyl sulfoxide; FITC, fluorescein isothiocyanate; SEM, standard error mean.

of vascular aggregates [Figure 9F (squares); $y = 7.566x + 17.19$, $r = 0.742$, $p = 0.014$].

Impact of the Chronic Fungicide Treatment on Gene and Protein Expression of Protagonists Involved in the Production or Clearance of Aβ Peptides

Because amyloid plaques and soluble forms of $A\beta_{1-42}$ were increased upon fungicide treatment (Figure 3B–E,H), we addressed whether cypro, mepa, and pyri could modulate either the production or the clearance of Aβ peptides. To this aim, we studied the gene and protein expression of the main protagonists of the amyloid cascade. First, total mRNA was extracted from brain homogenates of J20 mice treated with a cocktail of fungicides (T, $n = 4$) or with an equivalent volume of DMSO (CTR, $n = 4$) (Figure 1C, Study 2). The same procedure was performed for their WT littermates (CTR, $n = 3$; T, $n = 3$) (Figure 1C, Study 2). We analyzed mRNA expression of endogenous *App*, human *App*, *Bace1, Ide*, *Nep*, and *Lrp1* by RT-qPCR (see Figure S9A–F). No modifications of mRNA expression were observed for all the genes tested between fungicide-treated and DMSO-control

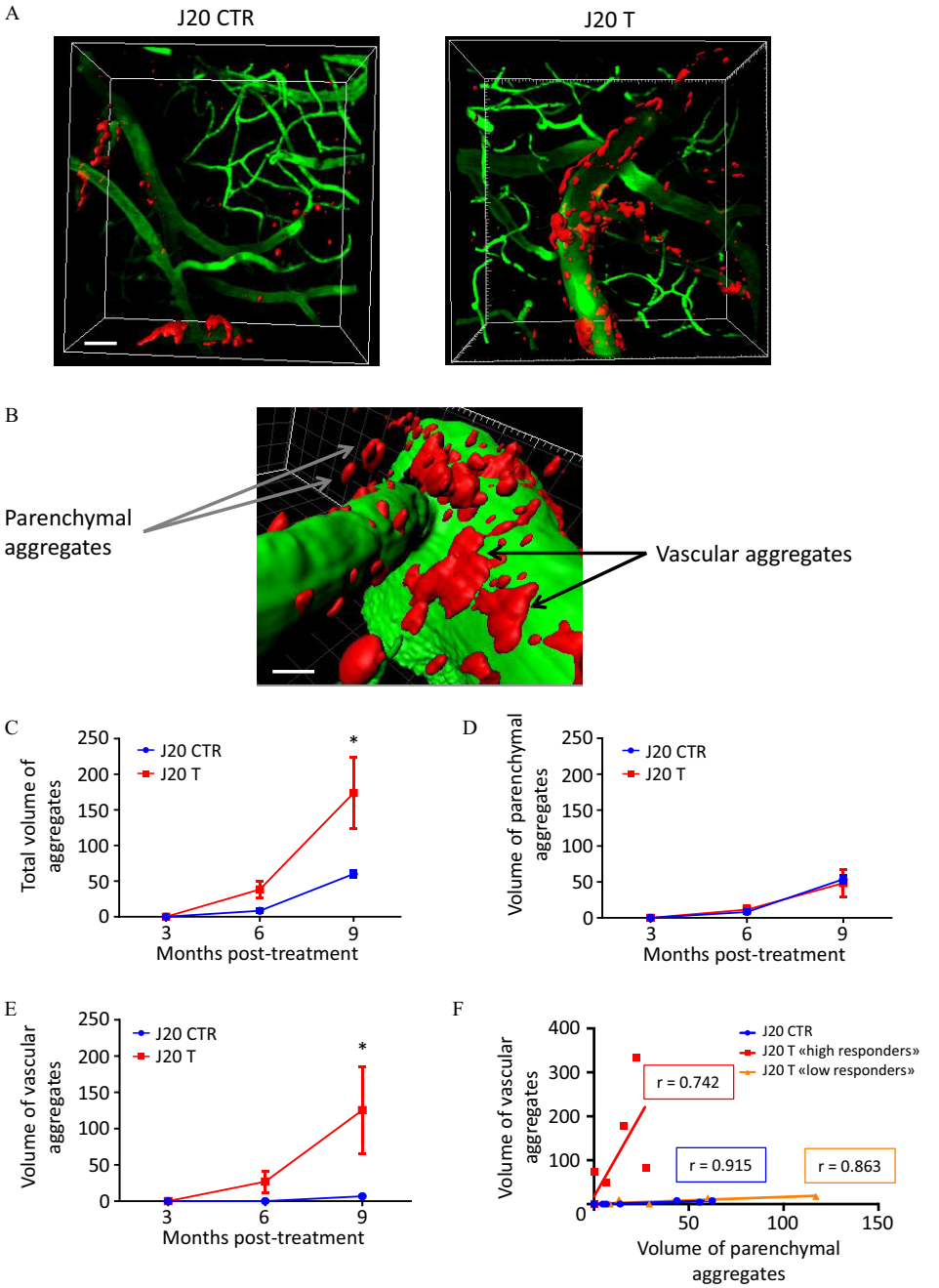

Figure 9. *In vivo* dynamics of amyloid plaque formation at 3, 6, and 9 months in the superficial cortex of J20 mice treated with (A) DMSO or fungicides, (B) 3D illustration of parenchymal and vascular aggregates, (C) quantification of the total, (D) parenchymal, and (E) vascular volume of aggregates, and (F) correlations with two subpopulations. (A) Representative 3D reconstructed images of J20 CTR and T mice at 9 months of treatment. (B) Example of a leptomeningeal vessel (in green) with vascular and parenchymal aggregates (artificially colored in red). Quantification of the (C) total, (D) parenchymal, and (E) vascular volume of aggregates was performed using Imaris software (version 5.0; Bitplane). Results were normalized by the total volume of the stack and multiplied by 10^5 to avoid decimal numbers. Quantifications were done at 3, 6, and 9 months of treatment and were presented as mean ± SEM (without unit). For statistical analysis a two-way ANOVA followed by a Holm-Sidak's post hoc analysis was used ($\alpha = 0.05$, $^*p < 0.05$). F. Linear correlation between the volumes of vascular and parenchymal aggregates of J20 CTR and T mice. In the J20 treated group two subpopulations were identified and referred to as low and high responders. Statistical significance was measured using a linear regression and Pearson's correlation coefficient (r). Scale bars: 40 µm. $n = 3$–5 animals per group issued from Study 3. Note: 3D, three dimensional; ANOVA, analysis of variance; CTR, control; DMSO, dimethyl sulfoxide; SEM, standard error mean; T, treatment.

mice. In parallel, we analyzed the expression of proteins corresponding to the genes cited above by immunoblotting. Analyses revealed a substantial increase of BACE1 expression in J20 mice treated with the cocktail of fungicides compared with the J20 CTR mice (Figure 10C; 0.762 ± 0.076 for J20 CTR vs. 1.323 ± 0.211 for J20 T, $p = 0.046$). In addition, NEP expression, one of the main clearance enzymes, was expressed in J20 mice treated with fungicides during 9 months at a level 50% of that of control-treated mice (Figure 10E; 0.274 ± 0.032 for J20 CTR vs. 0.141 ± 0.024 for J20 T, $p = 0.017$).

Discussion

Pesticides are widely used to preserve fields and harvests from pests. Their massive use since the 20th century has led to the

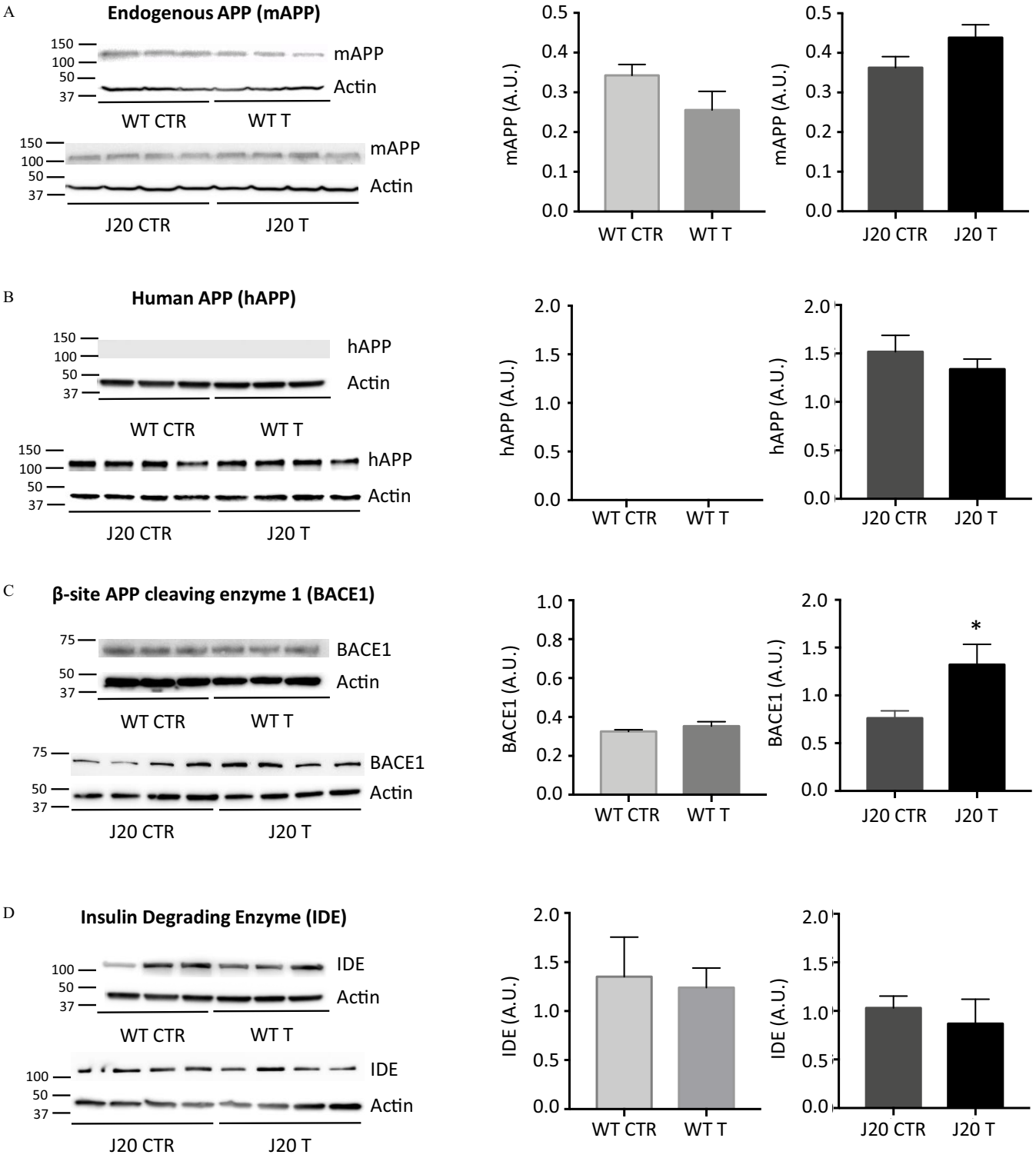

Figure 10. Protein expression levels of (A) mouse APP, (B) human APP, (C) BACE1, (D) IDE, (E) NEP, and (F) LRP1 for WT and J20 mice treated with DMSO or the cocktail of fungicides. Brain homogenates of WT and J20 animals, treated with the fungicide cocktail (0.1 μg/L each) (T) or with 3×10^{-5} % of DMSO (CTR) were used to measure protein levels of (A) mAPP, (B) hAPP, (C) BACE1, (D) IDE, (E) NEP, and (F) LRP1 by immunobloting. β-actin was used as a loading control. Membranes were revealed with a ChemiDoc MP Imager and signals were quantified on the Image Lab software (version 6.0.1; Biorad). All signal intensities were normalized to their respective β-actin signal. Results are presented as the mean ± SEM and statistical differences were analyzed using student's *t*-test ($\alpha = 0.05$, $^{*}p < 0.05$). $n = 3$–4 mice per group issued from Study 2. Note: A.U., arbitrary units; CTR, control; DMSO, dimethyl sulfoxide; hAPP, human amyloid precursor protein; mAPP, mouse amyloid precursor protein; SEM, standard error mean; T, treatment, WT, wild type.

contamination of all environmental media (water, soil, air), leading to residues in our diet. Although these compounds are present at very low concentrations (from nanograms to micrograms) in our environment (Table 1), the long-term effect of multiple pesticide residues on human health is subject to intense debate and concerns. Toxicological regulations are mainly based on high-dose effects and minimize the consequences of these traces. According to European institutions, pesticide residues can be consumed over a lifetime

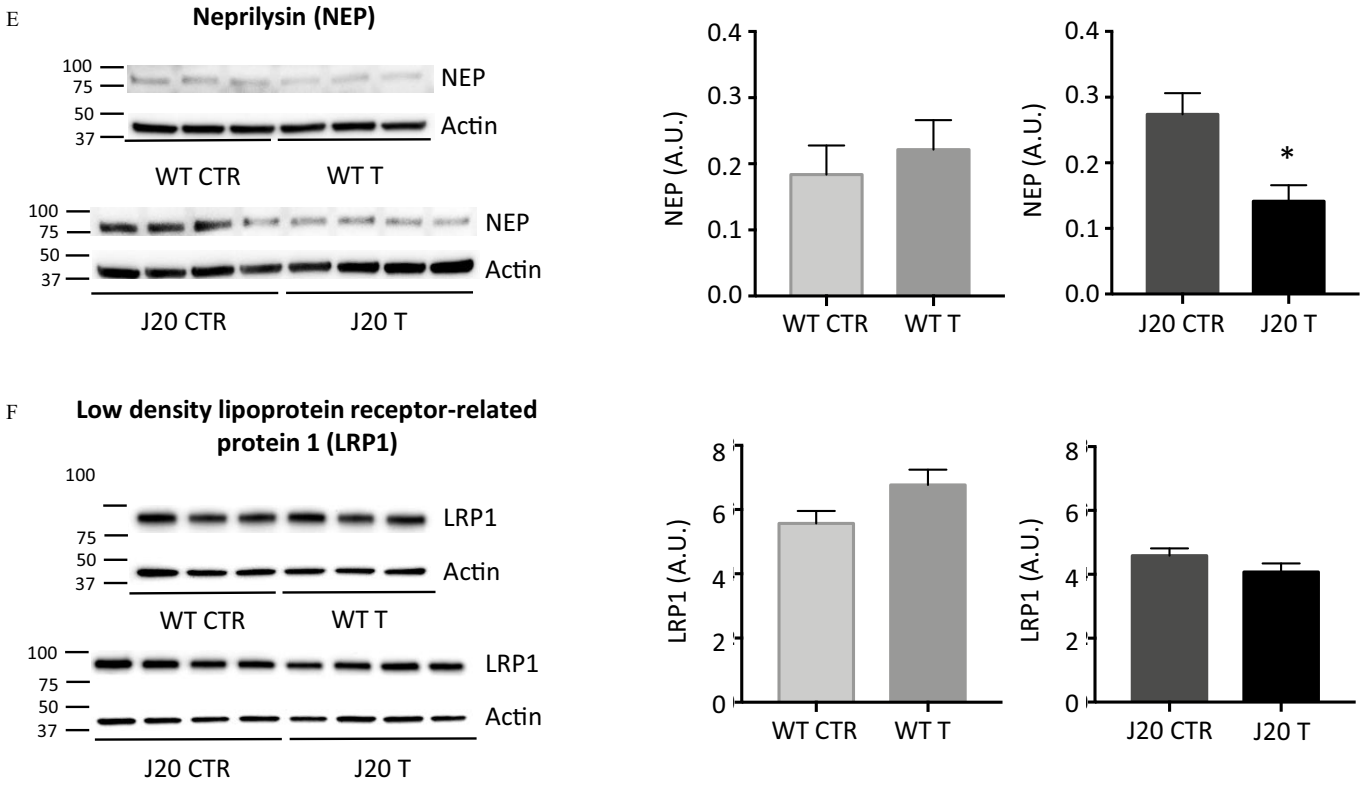

Figure 10. (*Continued.*)

without presenting a significant risk for human health (Council of the European Union 1998; EFSA 2017b, 2018, 2019). However, a study by Lukowicz et al. (2018) has demonstrated the impact of these chemical traces on human health. They showed that chronic dietary exposure to a cocktail of six commonly used pesticides in France, at the tolerable daily intake concentrations, had an obesogenic and diabetogenic effect on WT mice, treated for 52 weeks. Regarding neurodegenerative diseases, especially Alzheimer's disease, the link with pesticide residues is not clearly established, given that epidemiological studies can hardly associate a multiple chronic exposure to low doses of pollutants occurring throughout life and the pathology. However, Richardson et al. (2014) showed that DDE accumulated in the brains of 11 individuals with Alzheimer's disease although this herbicide has been prohibited since the 1970s. Furthermore, acute injections of chlorpyrifos (50 mg/kg) or paraquat (10 mg/kg twice a week for 3 weeks) to Tg2576 ($hAPP_{Sw}$) mice induced an increased production of Aβ peptides in the brain (Chen et al. 2012; Salazar et al. 2011). However, the doses and the route of treatment used in these *in vivo* studies are not relevant to the typical consumer's exposure to pesticides. To address the effect of pesticide residues in Alzheimer's disease, we used the J20 mouse model that had been chronically exposed to a cocktail of three fungicides (cypro, mepa, and pyri) through drinking water. Those residues are frequently detected in the European diet (Table 1). Mice were treated with 0.1 μg/L of each fungicide, leading to a final concentration of 0.3 μg/L in water. According to EU regulations, 0.1 μg/L corresponds to the maximal dose allowed for one pesticide in tap water and cannot exceed 0.5 μg/L for the presence of multiple residues (Council of the European Union 1998).

Limits of Detection and Quantification of Cypro, Mepa, and Pyri

The limits of detection (LOD) and quantification (LOQ) of these fungicides in water were respectively 0.019 and 0.063 μg/L for cypro [solid phase extraction–gas chromatography–mass spectrometry (SPE-GC-MS; Climent et al. 2018)]; 0.03 and 0.11 μg/L for mepa [single drop micro extraction (SDME)–GC-MS; Araujo et al. 2013], and 0.026 and 0.088 μg/L for pyri (SPE-GC-MS; Climent et al. 2018). In the present study, the dose used to treat WT and J20 animals was 0.1 μg/L for each fungicide, ranging from 444 to 502 pM. To detect such doses in an animal's brain, these fungicides should accumulate in this tissue and the detection of the nonmetabolized fungicides seems to be the limiting factor. Indeed, reports on mammalian toxicokinetics (absorption, distribution, excretion, and metabolism) of the three fungicides showed that these compounds were highly absorbed (80–95%) within 48 h and then highly excreted (EFSA 2006a, 2006b, 2017b). For example, cypro was extensively metabolized (EFSA 2006a) and up to 28 metabolites could be generated (FAO 2003). This compound was mainly excreted via urine (52–63%) and feces (33–45%), and only 3–8% of cypro was excreted unchanged in the feces (EFSA 2006a). The biodistribution of cypro in rats showed that there was no evidence of accumulation of this compound and <1% of the dose administered was found in tissues after 7 d of treatment (EFSA 2006a). The toxicokinetics of mepa and pyri were similar to those of cypro (EFSA 2006b, 2017b). In addition, toxicological reports did not indicate any data regarding the presence of these fungicides in brains in the different animals studied (e.g., cows, goats, rats, hens) (EFSA 2006a, 2006b, 2017b; FAO 2003, 2007). The presence of cypro, mepa, and pyri within amyloid plaques on brain tissue sections of J20 mice treated for 9 months with DMSO or with the cocktail of fungicides was assessed using anti-fungicide antibodies (see Figures S5 and S6). However, none of these fungicides could be detected in the amyloid plaques. The absence of labeling in this experiment could be explained either by the fact that these fungicides may not accumulate in brains and/or that compounds may be extensively metabolized. In addition, the anti-fungicide antibodies may not recognize metabolites. By contrast, the *ex vivo*

experiments (Figure 2A), lasting 1.5 h, allowed us to detect cypro, mepa, and pyri within amyloid plaques because the concentration of compounds was higher and a majority of nonmetabolized molecules were likely recognized by the antibodies. Mass spectrometry analyses would have been an alternative method to detect those fungicides. However, if we take into account the high rate of excretion of these fungicides, their nonaccumulation in tissues and their extensive rate of metabolization, the remaining concentration of the unchanged compounds may be barely detectable (i.e., <LOD) after a chronic treatment at 0.1 μg/L. In addition, the high number of possible metabolites for each compound 28 for cypro (FAO 2003), 4 for mepa (EFSA 2011), and 19 for pyri (FAO 2007) may further dilute the signal and increase the difficulties of detecting those compounds in brains.

Plaque Formation in the Hippocampus and the Cortex of J20 Mice Treated with the Fungicide Cocktail

Our results showed that a 9-month exposure to residues of cypro, mepa, and pyri (0.1 μg/L of each compound), mimicking a 20-y exposure in humans, induced a substantial increase in the number of amyloid plaques of about 26% and 53% in the hippocampus and the cortex of J20 mice, respectively (Figure 3B,D). Similarly, the treatment incremented the surface area of amyloid aggregates as well (hippocampus, ~42%; cortex, ~80%; Figure 3C,E). These results suggest that the three fungicides may interfere directly in the aggregation process, as suggested by our *in vitro* studies (Figure 2). As expected, WT mice did not exhibit ThT-positive aggregates [Figure 3A (left panel) and 3B–E], which was consistent with the literature as mouse Aβ aggregates are only visible from 15 months of age (Ahlemeyer et al. 2018). Moreover, our two-photon analysis revealed that the dynamics of Aβ aggregation in presence of fungicides occurred only between 6 and 9 months of treatment (Figure 8 and 9). Thus, it seems that the increase of amyloid aggregates in these conditions is dependent on preexisting amyloid plaques, possibly explaining the absence of ThT-positive aggregates in WT mice treated 9 months with fungicides. Remarkably, we showed that fungicides co-localized with amyloid plaques of J20 brain tissue sections after incubation, either alone or in cocktail, reflecting some affinity of these fungicides toward amyloid fibrils (Figure 2A). In addition, kinetics of amyloid fibril formation in presence of the three fungicides drastically reduced the lag phase and increased by more than 50% the ThT fluorescence intensity at the plateau, suggesting that the fibrils formed may have different structural characteristics (Figure 2B,C). After 100 h of incubation of $A\beta_{1–42}$ peptides with 30 μM of each fungicide (ratio 1:1) or with 750 μM of each fungicide (ratio 1:15), the kinetics reached the plateau phase, whereas the control curves had only begun their elongation phase, suggesting that these compounds promote a much faster nucleation than the control (Figure 2B,C). Our *in vitro* studies demonstrated a pro-aggregating effect of these fungicides. Remarkably, this process also occurred in J20 mice treated with concentrations as low as 444–502 pM (0.1 μg/L) (Figures 2 and 3). Brain homogenates analyses also showed that J20 treated mice presented almost three times more soluble human $A\beta_{1–42}$ levels than the control group (Figure 3H). Because the kinetics of fibril formation started nearly immediately in the presence of fungicides (Figure 2B,C), we hypothesize that this increased soluble human $A\beta_{1–42}$ fractions found *in vivo* may be composed mainly of soluble oligomeric species, rather than monomers. The substantial increase of Aβ species upon treatment may be related to the higher levels of BACE1 (Figure 10C) and lower levels of NEP proteins (Figure 10E). We speculate that the higher levels of BACE1 may increase β-cleavage of APP and lower levels of NEP may result in a decrease in clearance of amyloid peptides, thus facilitating accumulation of Aβ species. Our results are in agreement with a recent study showing the effect of six triazine herbicides on β- and γ-secretases associated with an overproduction of $A\beta_{1–42}$ peptides on inducible pluripotent stem cells (iPSCs) derived from patients with familial Alzheimer's disease (Portelius et al. 2016). Regarding WT mice, no differences were observed in protein expression levels for the different protagonists involved in the amyloid cascade (Figure 10A–F), possibly explaining why we did not observe the presence of amyloid plaques in WT mice after 9 months of fungicide treatment (Figure 3A–E).

Cerebral Amyloid Angiopathy upon Fungicide Cocktail Treatment

Because we did not know when the pro-aggregative effect of these fungicides started in the J20 treated mice, we carried out a longitudinal study at 3, 6, and 9 months by two-photon microscopy (Figures 8 and 9). Analyses of the different time points revealed that treatment of J20 mice with fungicides *a*) increased amyloid plaque formation between 6 and 9 months, *b*) caused a substantial augmentation of vascular amyloid plaques reminiscent to cerebral amyloid angiopathy (CAA), and *c*) had no effect on parenchymal aggregates of the superficial cortex. In addition, in the J20 fungicide-treated group, the highlighting of the low responders and the high responders subpopulations implied an interindividual susceptibility to pesticide residues exposure toward CAA (Figure 9F). We thus can hypothesize that this sensitivity toward low doses of fungicides may also exist in humans. Analysis of the 3D reconstructed images also showed that vascular aggregates were placed on the blood vessel walls and may not cross them, except for one aggregate that was found inside a blood vessel at 6 months of treatment and disappeared at 9 months (see Figure S8). These results suggest that the enhanced CAA observed in J20 treated mice could also be related to defects in the peri-arterial interstitial fluid drainage pathway to eliminate the surplus of aggregates (Yoon and AhnJo 2012). This striking effect on the CAA is likely linked to the disruption of the blood–brain barrier (BBB) in J20 mice (Kimbrough et al. 2015), likely facilitating the entrance of cypro, mepa, and pyri into the central nervous system (CNS). A toxicological report showed that oral treatment of a cow with pyri (0.4 mg/kg body weight per day for 7 d) resulted in the detection of 34 μg of metabolites in the blood (FAO 2007). Results were similar for the biodistribution of pyri metabolites when treatment was applied to rats (FAO 2007). Altogether, these toxicological data demonstrate that these fungicides and their metabolites circulate in the blood and thus can reach the brain. In addition, studies on J20 mice showed that CAA deposits disrupted the normal contact of astrocytic end-feet with vessels, thus damaging the BBB (Kimbrough et al. 2015). This disruption is an open window for pesticides to reach CNS and strengthen CAA. Our results are in accordance with the permeability of the BBB of the J20 model. Previous studies showed that β-amyloid deposits formed a physical cast, making blood vessels more rigid and unable to constrict and dilate as do vessels free of amyloid and leading to vascular pathologies (Kimbrough et al. 2015). In this context, one can hypothesize that the chronic exposure to those fungicide residues of patients already having a permeability of the BBB and an altered gliovascular unit could result in an aggravation of vascular deposits. These deposits could lead ultimately to CAA-associated intracerebral hemorrhages, a known comorbidity of Alzheimer's disease that often leads to cognitive impairments (Shi et al. 2000).

Neuroinflammation Processes upon Fungicide Treatment in J20 Treated Mice

Neuroinflammation processes are one of the hallmarks of Alzheimer's disease and is associated with the presence of both activated astrocytes and microglia. GFAP is the typical marker used to analyze the

activation of astrocytes and their morphological changes (Eng et al. 1992). IBA1 allows the study of changes in microglial cells from a ramified state (quiescent) to an activated state (ameboid) (Ito et al. 1998). A previous study revealed that J20 mice exhibited a peak of astrogliosis in the hippocampus at 6 months of age while activated microglial cells increased over time (Wright et al. 2013). Our results showed that J20 mice treated with fungicides exhibited higher astrogliosis (DG, CA1, Figure 4), as well as higher activated microglial cells in the different regions of the hippocampus upon 9 months of fungicide treatment (Figure 5). In a study of 40 postmortem brains of patients with Alzheimer's disease, Serrano-Pozo et al. (2011) found more activated microglia near amyloid plaques ($\leq$50 μm) than distant to the plaques. Authors speculated that this finding may imply that amyloid plaques could be involved in the activation of microglial cells (Serrano-Pozo et al. 2011). Augmentation of amyloid aggregates in the hippocampus of J20 mice treated with fungicides (Figure 3) may participate in the increased number of ameboid forms of microglia given that higher clusters around amyloid plaques were observed in the DG (Figure 5A, row 1). Moreover, we also measured a greater number of the pro-inflammatory interleukins IL1β and IL6 in the brains of J20 mice treated with fungicides compared with J20 mice treated with vehicle (Figure 6A–B). These two interleukins have been shown to contribute to neuronal death. Indeed, IL1β was shown to induce neuronal cell death when recombinant IL1β treatment (0.01–100 ng/mL) was applied in a glial–neuronal coculture extracted from rat embryos (Thornton et al. 2006). By contrast, IL6 had a dual effect: In physiological conditions, IL6 was involved in adult neurogenesis (Deverman and Patterson 2009) as well as in cell survival (Hama et al. 1989); however, in pathological conditions, IL6 can contribute to neuronal cell death, associated with other factors. A study showed that cortical neurons extracted from rat embryos, treated with IL6 (5 ng/mL), can have an effect only when combined with $A\beta_{25–35}$ peptides (20 μM), by increasing cell damage (LDH assay) and by decreasing cell survival (MTT assay) (Qiu and Gruol 2003). The higher levels of IL1β and IL6 detected in the J20 mice treated with fungicides may explain the neuronal cell death observed in the CA3 area of these mice (Figure 7E). In addition, activation of IL1β, IL6, and TNFα receptors has been described to activate NFκB and AP-1 transcription factors (Figure 6 of Cronin et al. 2016; Jain et al. 2014; Shi and Sun 2018). Interestingly, NFκB and AP-1 can activate the transcription of BACE1 (Chami and Checler 2012), which could explain, in part, the increased expression of the β-secretase in the J20 mice treated with fungicides but not in their WT littermates (Figure 10C). So we could imagine a vicious circle where the fungicides could induce more amyloid aggregates, which in turn would produce more inflammatory processes. We can then hypothesize that the activation of microglia and astrocytes could lead to a secretion of pro-inflammatory interleukins, emphasizing BACE1 expression and ultimately leading to an increased production of $A\beta_{1–42}$ peptides. Thus, in the presence of the fungicides, $A\beta_{1–42}$ peptides may aggregate faster, producing higher and larger amyloid plaques and thus exacerbating, again, inflammatory processes.

Conclusions

To our knowledge, our study is the first one demonstrating the effect of very low doses of fungicides in the aggravation of Alzheimer's disease markers in a transgenic mouse model reminiscent of familial cases. Because the fungicides we studied exacerbated amyloid fibril formation, amyloid plaques, and inflammatory processes, we can suspect that they may also corrupt normal brain aging and aggravate the markers of sporadic Alzheimer's disease cases. For this purpose, future studies will be carried out on a mouse model expressing WT human APP to decipher whether treatment with fungicides could also have a causal effect in Alzheimer's disease. According to the EU, such low doses in water (0.1 μg/L) have been selected to "ensure that water intended for human consumption can be consumed safely on a lifelong basis and thus represent a high level of health protection" (Council of the European Union 1998). However, our results showed that these doses, on the long term, are deleterious in a transgenic mouse model of Alzheimer's disease. Cypro, mepa, and pyri could be considered Alzheimerogen pollutants (Cam et al. 2018; Portelius et al. 2016) at the subnanomolar regulatory levels (0.1 μg/L) because they accelerated fibrils formation and promoted the progression of disease's markers in the J20 mouse model. We hypothesize that prevention strategies toward pesticide long-term exposure may be an alternative to counterbalance the lack of treatment and to slow down the worldwide Alzheimer's epidemic.

Acknowledgments

P.A.L. and V.P. conceived the study, participated in its design and interpretation and wrote the manuscript. P.A.L., Y.W., J.T., M.A.L., L.S.P., M.M., C.D., and V.P. performed the experiments and analyzed data. J.V.M. provided antibodies against cyprodinil, mepanipyrim, and pyrimethanil. N.M.F., C.D., and L.G. provided protocols and advice for histological studies. F.J., J.T., L.S.P., and J.L. provided constructive criticisms for manuscript. All authors read and approved the final manuscript.

We acknowledge the imaging facility Montpellier Ressources Imagerie (MRI), member of the national infrastructure France-BioImaging infrastructure supported by the French National Research Agency (ANR-10-INBS-04, Investments for the Future). We thank V. Diakou and E. Jublanc for their help in image acquisition and analysis. We also thank M.-P. Cabrera (Animalerie CECEMA, Montpellier) and E. Huetter for their technical assistance and advice. We thank the CISBIO Bioassays Research and Development team (T. Roux, S. Bdioui, and S. Junique) for their technical assistance on homogeneous time resolved fluorescence technology.

This project was supported by the French government under the Programme d'investissement d'Avenir, Initiative Sciences Innovation Territoire–MUSE (Montpellier University Site of Excellence) with reference ANR-16-IDEX-0006, I-Site MUSE STEMPest. This project was supported by grants from the French National Research Agency (ANR) under the program Investissement d'Avenir with reference ANR-11-LABX-0021-LipSTIC. W.Y. is the recipient of a fellowship from the China Scholarship Council under the Programme Hubert Curien (PHC) CAI YUANPEI 2014-16–project no. 32106RD and a joint-PhD student from Huazhong University of Science and Technology and University of Montpellier. P.A.L. is the recipient of a fellowship from the French Ministry of Higher Education and Research and from the Center of Excellence for Neurodegenerative diseases of Montpellier (CoEN)–CHU of Montpellier certified by AVIESAN as part of the Plan maladies neurodégénératives (2014–2019).

References

Ahlemeyer B, Halupczok S, Rodenberg-Frank E, Valerius K-P, Baumgart-Vogt E. 2018. Endogenous murine amyloid-β peptide assembles into aggregates in the aged C57BL/6J mouse suggesting these animals as a model to study pathogenesis of amyloid-β plaque formation. J Alzheimers Dis 61(4):1425–1450, PMID: 29376876, https://doi.org/10.3233/JAD-170923.

ANSES (Agence Nationale de SEcurité Sanitaire de l'alimentation, de l'environnement et du travail). 2010. Recommandations et perspectives pour une surveillance nationale de la contamination de l'air par les pesticides. Synthèse et recommandations du comité d'orientation et de prospective scientifique de l'observatoire des résidus de pesticides (ORP). [In French.] Rapport scientifique. https://www.anses.fr/en/system/files/ORP-Ra-2010AirPesticide.pdf [accessed 29 December 2019].

ANSES. 2011. Second French Total Diet Study (TDS2). Report 2. Pesticide residues, additives, acrylamide and polycyclic aromatic hydrocarbons. ANSES Opinion. https://www.anses.fr/en/system/files/PASER2006sa0361Ra2EN.pdf [accessed 29 December 2019].
ANSES. 2013. Évaluation des risques liés aux résidus de pesticides dans l'eau de distribution. Contribution à l'exposition alimentaire totale. Rapport d'étude scientifique. [In French.] https://www.anses.fr/fr/system/files/ORP-Ra-PesticidesEau.pdf [accessed 29 December 2019].
Arango-Lievano M, Giannoni P, Claeysen S, Marchi N, Jeanneteau F. 2016. Longitudinal *in vivo* imaging of the cerebrovasculature: relevance to CNS diseases. J Vis Exp 118:e54796, PMID: 28060355, https://doi.org/10.3791/54796.
Araujo L, Troconis ME, Cubillán D, Mercado J, Villa N, Prieto A. 2013. Single drop microextraction and gas chromatography–mass spectrometry for the determination of diflufenican, mepanipyrim, fipronil, and pretilachlor in water samples. Environ Monit Assess 185(12):10225–10233, PMID: 23887887, https://doi.org/10.1007/s10661-013-3327-8.
Bermúdez-Couso A, Arias-Estévez M, Nóvoa-Muñoz JC, López-Periago E, Soto-González B, Simal-Gándara J. 2007. Seasonal distributions of fungicides in soils and sediments of a small river basin partially devoted to vineyards. Water Res 41(19):4515–4525, PMID: 17624393, https://doi.org/10.1016/j.watres.2007.06.029.
Bustin SA, Benes V, Garson JA, Hellemans J, Huggett J, Kubista M, et al. 2009. The MIQE guidelines: *M*inimum *I*nformation for publication of *Q*uantitative real-time PCR *E*xperiments. Clin Chem 55(4):611–622, PMID: 19246619, https://doi.org/10.1373/clinchem.2008.112797.
Cai H, Wang Y, McCarthy D, Wen H, Borchelt DR, Price DL, et al. 2001. BACE1 is the major β-secretase for generation of Aβ peptides by neurons. Nat Neurosci 4(3):233–234, PMID: 11224536, https://doi.org/10.1038/85064.
Cam M, Durieu E, Bodin M, Manousopoulou A, Koslowski S, Vasylieva N, et al. 2018. Induction of amyloid-β42 production by fipronil and other pyrazole insecticides. J Alzheimers Dis 62(4):1663–1681, PMID: 29504531, https://doi.org/10.3233/JAD-170875.
Carroll CM, Li Y-M. 2016. Physiological and pathological roles of the γ-secretase complex. Brain Res Bull 126(Pt 2):199–206, PMID: 27133790, https://doi.org/10.1016/j.brainresbull.2016.04.019.
Chami L, Checler F. 2012. BACE1 is at the crossroad of a toxic vicious cycle involving cellular stress and β-amyloid production in Alzheimer's disease. Mol Neurodegener 7:52, PMID: 23039869, https://doi.org/10.1186/1750-1326-7-52.
Chen L, Yoo S-E, Na R, Liu Y, Ran Q. 2012. Cognitive impairment and increased Aβ levels induced by paraquat exposure are attenuated by enhanced removal of mitochondrial H_2O_2. Neurobiol Aging 33(2):432.e15–432.e26, PMID: 21429624, https://doi.org/10.1016/j.neurobiolaging.2011.01.008.
Chin-Chan M, Segovia J, Quintanar L, Arcos-López T, Hersh LB, Chow KM, et al. 2015. Mercury reduces the enzymatic activity of neprilysin in differentiated SH-SY5Y cells. Toxicol Sci 145(1):128–137, PMID: 25673500, https://doi.org/10.1093/toxsci/kfv037.
Climent MJ, Sánchez-Martín MJ, Rodríguez-Cruz MS, Pedreros P, Urritia R, Herrero-Hernández E. 2018. Determination of pesticides in river surface waters of central Chile using SPE-GC-MS multi-residue method. J Chil Chem Soc 63(2):4023–4031, https://doi.org/10.4067/s0717-97072018000204023.
Council of the European Union. 1998. Council directive 98/83EC of 3 November 1998 on the quality of water for human consumption. Off J Eur Communities L 330:32–54.
Cronin JG, Kanamarlapudi V, Thornton CA, Sheldon IM. 2016. Signal transducer and activator of transcription-3 licenses Toll-like receptor 4-dependent interleukin (IL)-6 and IL-8 production via IL-6 receptor-positive feedback in endometrial cells. Mucosal Immunol 9(5):1125–1136, PMID: 26813342, https://doi.org/10.1038/mi.2015.131.
Désert M, Ravier S, Gille G, Quinapallo A, Armengaud A, Pochet G, et al. 2018. Spatial and temporal distribution of current-use pesticides in ambient air of Provence-Alpes-Côte-d'Azur Region and Corsica, France. Atmos Environ 192:241–256, https://doi.org/10.1016/j.atmosenv.2018.08.054.
Deverman BE, Patterson PH. 2009. Cytokines and CNS development. Cell 64(1):61–78, PMID: 19840550, https://doi.org/10.1016/j.neuron.2009.09.002.
EFSA (European Food Safety Authority). 2006a. Conclusion regarding the peer review of the pesticide risk assesment of the active substance cyprodinil. EFSA J 4(1):RN-51, https://doi.org/10.2903/j.efsa.2006.51r.
EFSA. 2006b. Conclusion regarding the peer review of the pesticide risk assessment of the active substance pyrimethanil. EFSA J 4(2):RN-61, https://doi.org/10.2903/j.efsa.2006.61r.
EFSA. 2011. Review of the existing maximum residue levels (MRLs) for mepanipyrim according to Article 12 of Regulation (EC) No 396/2005. EFSA J 9(8):2342, https://doi.org/10.2903/j.efsa.2011.2342.
EFSA. 2017a. Peer review of the pesticide risk assessment of the active substance mepanipyrim. EFSA J 15(6):4852, https://doi.org/10.2903/j.efsa.2017.4852.
EFSA. 2017b. The 2015 European Union report on pesticide residues in food. EFSA J 15(4):4791, https://doi.org/10.2903/j.efsa.2017.4791.
EFSA. 2018. The 2016 European Union report on pesticide residues in food. EFSA J 16(7):5348, https://doi.org/10.2903/j.efsa.2018.5348.
EFSA. 2019. The 2017 European Union report on pesticide residues in food. EFSA J 17(6):5743, https://doi.org/10.2903/j.efsa.2019.5743.
Eng LF, Yu AC, Lee YL. 1992. Astrocytic response to injury. Prog Brain Res 94:353–365, PMID: 1337615, https://doi.org/10.1016/s0079-6123(08)61764-1.
Esteve-Turrillas FA, Agulló C, Abad-Fuentes A, Abad-Somovilla A, Mercader JV. 2012. Immunoreagent generation and competitive assay development for cyprodinil analysis. J Agric Food Chem 60(19):4803–4811, PMID: 22500467, https://doi.org/10.1021/jf300319n.
Esteve-Turrillas FA, Mercader JV, Agulló C, Abad-Somovilla A, Abad-Fuentes A. 2013. Mepanipyrim haptens and antibodies with nanomolar affinity. Analyst 138(12):3360–3364, PMID: 23666476, https://doi.org/10.1039/c3an00228d.
FAO (Food and Agriculture Organization of the United Nations). 2003. Cyprodinil: a first draft prepared by David Hamilton. FAO reports, p169–187. http://www.fao.org/fileadmin/templates/agphome/documents/Pests_Pesticides/JMPR/Evaluation03/Cyprodinil_2003.pdf [accessed 29 December 2019].
FAO. 2007. Pyrimethanil (226): a first draft prepared by Stephen Funk. FAO reports, p 919–1022. http://www.fao.org/fileadmin/templates/agphome/documents/Pests_Pesticides/JMPR/Evaluation07/Pyrimethanil.pdf [accessed 29 December 2019].
Fathabadi B, Dehghanifiroozabadi M, Aaseth J, Sharifzadeh G, Nakhaee S, Rajabpour-Sanati A, et al. 2018. Comparison of blood lead levels in patients with Alzheimer's disease and healthy people. Am J Alzheimers Dis Other Demen 33(8):541–547, PMID: 30134734, https://doi.org/10.1177/1533317518794032.
Générations Futures. 2013. *Enquête EXPPERT II: des pesticides interdits et des perturbateurs endocriniens (PE) dans des fraises*. [In French.] https://www.generations-futures.fr/wp-content/uploads/2013/07/EXPPERT-2-fraises-final.pdf [accessed 29 December 2019].
Générations Futures. 2016a. Enquête EXPPERT 7: des pesticides perturbateurs endocriniens dans des mueslis. [In French.] https://www.generations-futures.fr/wp-content/uploads/2016/10/Enquete_7_final.pdf [accessed 29 December 2019].
Générations Futures. 2016b. Enquête EXPPERT 6 (analyse des poussières): des riverains de zones cultivées exposés aux pesticides perturbateurs endocriniens chez eux, tout au long de l'année. [In French.] https://www.generations-futures.fr/wp-content/uploads/2016/03/EXPPERT-6-Final.pdf [accessed 29 December 2019].
Générations Futures. 2017. Enquête EXPPERT 9: exposition aux perturbateurs endocriniens, 7 personnalités de l'écologie font analyser leurs cheveux. [In French.] https://www.generations-futures.fr/wp-content/uploads/2017/02/EXPPERT-9-FV-220216.pdf [accessed 29 December 2019].
Giannoni P, Arango-Lievano M, Neves ID, Rousset M-C, Baranger K, Rivera S, et al. 2016. Cerebrovascular pathology during the progression of experimental Alzheimer's disease. Neurobiol Dis 88:107–117, PMID: 26774030, https://doi.org/10.1016/j.nbd.2016.01.001.
Gu H, Wei X, Monnot AD, Fontanilla CV, Behl M, Farlow MR, et al. 2011. Lead exposure increases levels of β-amyloid in the brain and CSF and inhibits LRP1 expression in APP transgenic mice. Neurosci Lett 490(1):16–20, PMID: 21167913, https://doi.org/10.1016/j.neulet.2010.12.017.
Hama T, Miyamoto M, Tsukui H, Nishio C, Hatanaka H. 1989. Interleukin-6 as a neurotrophic factor for promoting the survival of cultured basal forebrain cholinergic neurons from postnatal rats. Neurosci Lett 104(3):340–344, PMID: 2812549, https://doi.org/10.1016/0304-3940(89)90600-9.
Hayden KM, Norton MC, Darcey D, Ostbye T, Zandi PP, Breitner JCS, et al. 2010. Occupational exposure to pesticides increases the risk of incident AD: the Cache County study. Neurology 74(19):1524–1530, PMID: 20458069, https://doi.org/10.1212/WNL.0b013e3181dd4423.
Herrero-Hernández E, Pose-Juan E, Sánchez-Martín MJ, Andrades MS, Rodríguez-Cruz MS. 2016. Intra-annual trends of fungicide residues in waters from vineyard areas in La Rioja region of northern Spain. Environ Sci Pollut Res Int 23(22):22924–22936, PMID: 27578090, https://doi.org/10.1007/s11356-016-7497-0.
Huang H, Bihaqi SW, Cui L, Zawia NH. 2011. *In vitro* Pb exposure disturbs the balance between Aβ production and elimination: the role of AβPP and neprilysin. Neurotoxicology 32(3):300–306, PMID: 21315759, https://doi.org/10.1016/j.neuro.2011.02.001.
Ito D, Imai Y, Ohsawa K, Nakajima K, Fukuuchi Y, Kohsaka S. 1998. Microglia-specific localisation of a novel calcium binding protein, Iba1. Brain Res Mol Brain Res 57(1):1–9, PMID: 9630473, https://doi.org/10.1016/S0169-328X(98)00040-0.
Iwatsubo T, Odaka A, Suzuki N, Mizusawa H, Nukina N, Ihara Y. 1994. Visualization of Aβ42(43) and Aβ40 in senile plaques with end-specific Aβ monoclonals: evidence that an initially deposited species is Aβ42(43). Neuron 13(1):45–53, PMID: 8043280, https://doi.org/10.1016/0896-6273(94)90458-8.
Jain A, Kaczanowska S, Davila E. 2014. IL-1 receptor-associated kinase signaling and its role in inflammation, cancer progression, and therapy resistance. Front Immunol 5:553, PMID: 25452754, https://doi.org/10.3389/fimmu.2014.00553.

Kang DE, Pietrzik CU, Baum L, Chevallier N, Merriam DE, Kounnas MZ, et al. 2000. Modulation of amyloid β-protein clearance and Alzheimer's disease susceptibility by the LDL receptor–related protein pathway. J Clin Invest 106(9):1159–1166, PMID: 11067868, https://doi.org/10.1172/JCI11013.

Kawahara M, Kato M, Kuroda Y. 2001. Effects of aluminum on the neurotoxicity of primary cultured neurons and on the aggregation of β-amyloid protein. Brain Res. Bull 55(2):211–217, PMID: 11470317, https://doi.org/10.1016/S0361-9230(01)00475-0.

Kim D-K, Park J-D, Choi B-S. 2014. Mercury-induced amyloid-beta (Aβ) accumulation in the brain is mediated by disruption of Aβ transport. J Toxicol Sci 39(4):625–635, PMID: 25056787, https://doi.org/10.2131/jts.39.625.

Kimbrough IF, Robel S, Roberson ED, Sontheimer H. 2015. Vascular amyloidosis impairs the gliovascular unit in a mouse model of Alzheimer's disease. Brain 138(Pt 12):3716–3733, PMID: 26598495, https://doi.org/10.1093/brain/awv327.

Lafon P-A, Imberdis T, Wang Y, Torrent J, Robitzer M, Huetter E, et al. 2018. Low doses of bioherbicide favour prion aggregation and propagation *in vivo*. Sci. Rep 8(1):8023, PMID: 29795181, https://doi.org/10.1038/s41598-018-25966-9.

Lukowicz C, Ellero-Simatos S, Régnier M, Polizzi A, Lasserre F, Montagner A, et al. 2018. Metabolic effects of a chronic dietary exposure to a low-dose pesticide cocktail in mice: sexual dimorphism and role of the constitutive androstane receptor. Environ Health Perspect 126(6):067007, PMID: 29950287, https://doi.org/10.1289/EHP2877.

Luo Y, Bolon B, Bennett BD, Babu-Khan S, Denis P, Fan W, et al. 2001. Mice deficient in BACE1, the Alzheimer's β-secretase, have normal phenotype and abolished β-amyloid generation. Nat Neurosci 4(3):231–232, PMID: 11224535, https://doi.org/10.1038/85059.

Mansuy M, Baille S, Canet G, Borie A, Cohen-Solal C, Vignes M, et al. 2018. Deletion of plasma *Phospholipid Transfer Protein* (*PLTP*) increases microglial phagocytosis and reduces cerebral amyloid-β deposition in the J20 mouse model of Alzheimer's disease. Oncotarget 9(28):19688–19703, PMID: 29731975, https://doi.org/10.18632/oncotarget.24802.

Mercader JV, Esteve-Turrillas FA, Agulló C, Abad-Somovilla A, Abad-Fuentes A. 2012. Antibody generation and immunoassay development in diverse formats for pyrimethanil specific and sensitive analysis. Analyst 137(23):5672–5679, PMID: 23085609, https://doi.org/10.1039/c2an35801h.

Miners JS, Baig S, Tayler H, Kehoe PG, Love S. 2009. Neprilysin and insulin-degrading enzyme levels are increased in Alzheimer disease in relation to disease severity. J Neuropathol Exp Neurol 68(8):902–914, PMID: 19606063, https://doi.org/10.1097/NEN.0b013e3181afe475.

Miners JS, Van Helmond Z, Chalmers K, Wilcock G, Love S, Kehoe PG. 2006. Decreased expression and activity of neprilysin in Alzheimer disease are associated with cerebral amyloid angiopathy. J Neuropathol Exp Neurol 65(10):1012–1021, PMID: 17021406, https://doi.org/10.1097/01.jnen.0000240463.87886.9a.

Mucke L, Masliah E, Yu GQ, Mallory M, Rockenstein EM, Tatsuno G, et al. 2000. High-level neuronal expression of $A\beta_{1-42}$ in wild-type human amyloid protein precursor transgenic mice: synaptotoxicity without plaque formation. J Neurosci 20(11):4050–4058, PMID: 10818140, https://doi.org/10.1523/JNEUROSCI.20-11-04050.2000.

Mura T, Dartigues J-F, Berr C. 2010. How many dementia cases in France and Europe? Alternative projections and scenarios 2010–2050. Eur J Neurol 17(2):252–259, PMID: 19796284, https://doi.org/10.1111/j.1468-1331.2009.02783.x.

Nasri A, Valverde AJ, Roche DB, Desrumaux C, Clair P, Beyrem H, et al. 2016. Neurotoxicity of a biopesticide analog on zebrafish larvae at nanomolar concentrations. Int J Mol Sci 17(12):E2137, PMID: 27999363, https://doi.org/10.3390/ijms17122137.

O'Brien RJ, Wong PC. 2011. Amyloid precursor protein processing and Alzheimer's disease. Annu Rev Neurosci 34:185–204, PMID: 21456963, https://doi.org/10.1146/annurev-neuro-061010-113613.

OECD (Organisation for Economic Co-operation and Development). 2018. *Care Needed: Improving the Lives of People with Dementia*. OECD Health Policy Studies. Paris, France: OECD Publishing.

PAN Europe (Pesticide Action Network). 2008. *Etude vin de PAN-Europe/MDRGF*. Etude sur la présence de résidus de pesticides dans le vin. [In French.] https://www.generations-futures.fr/wp-content/uploads/2017/05/rapport_vin_pesticide_fr.pdf [accessed 29 December 2019].

Portelius E, Durieu E, Bodin M, Cam M, Pannee J, Leuxe C, et al. 2016. Specific triazine herbicides induce amyloid-β42 production. J Alzheimers Dis 54(4):1593–1605, PMID: 27589520, https://doi.org/10.3233/JAD-160310.

Qiu Z, Gruol DL. 2003. Interleukin-6, β-amyloid peptide and NMDA interactions in rat cortical neurons. J Neuroimmunol 139(1–2):51–57, PMID: 12799020, https://doi.org/10.1016/s0165-5728(03)00158-9.

Rial-Otero R, González-Rodríguez RM, Cancho-Grande B, Simal-Gándara J. 2004. Parameters affecting extraction of selected fungicides from vineyard soils. J Agric Food Chem 52(24):7227–7234, PMID: 15563199, https://doi.org/10.1021/jf0493019.

Richardson JR, Roy A, Shalat SL, von Stein RT, Hossain MM, Buckley B, et al. 2014. Elevated serum pesticide levels and risk for Alzheimer disease. JAMA Neurol 71(3):284–290, PMID: 24473795, https://doi.org/10.1001/jamaneurol.2013.6030.

Salazar JG, Ribes D, Cabré M, Domingo JL, Sanchez-Santed F, Colomina MT. 2011. Amyloid β peptide levels increase in brain of AβPP Swedish mice after exposure to chlorpyrifos. Curr Alzheimer Res 8(7):732–740, PMID: 21592053, https://doi.org/10.2174/156720511797633197.

Serra-Batiste M, Ninot-Pedrosa M, Bayoumi M, Gairí M, Maglia G, Carulla N. 2016. Aβ42 assembles into specific β-barrel pore-forming oligomers in membrane-mimicking environments. Proc Natl Acad Sci USA 113(39):10866–10871, PMID: 27621459, https://doi.org/10.1073/pnas.1605104113.

Serrano-Pozo A, Mielke ML, Gómez-Isla T, Betensky RA, Growdon JH, Frosch MP, et al. 2011. Reactive glia not only associates with plaques but also parallels tangles in Alzheimer's disease. Am J Pathol 179(3):1373–1384, PMID: 21777559, https://doi.org/10.1016/j.ajpath.2011.05.047.

Shi J, Perry G, Smith MA, Friedland RP. 2000. Vascular abnormalities: the insidious pathogenesis of Alzheimer's disease. Neurobiol Aging 21(2):357–361, PMID: 10867221, https://doi.org/10.1016/S0197-4580(00)00119-6.

Shi J-H, Sun S-C. 2018. Tumor necrosis factor receptor-associated factor regulation of nuclear factor κB and mitogen-activated protein kinase pathways. Front Immunol 9:1849, PMID: 30140268, https://doi.org/10.3389/fimmu.2018.01849.

Shinohara M, Fujioka S, Murray ME, Wojtas A, Baker M, Rovelet-Lecrux A, et al. 2014. Regional distribution of synaptic markers and APP correlate with distinct clinicopathological features in sporadic and familial Alzheimer's disease. Brain 137(Pt 5):1533–1549, PMID: 24625695, https://doi.org/10.1093/brain/awu046.

Thornton P, Pinteaux E, Gibson RM, Allan SM, Rothwell NJ. 2006. Interleukin-1-induced neurotoxicity is mediated by glia and requires caspase activation and free radical release. J Neurochem 98(1):258–266, PMID: 16805812, https://doi.org/10.1111/j.1471-4159.2006.03872.x.

Walton JR, Wang M-X. 2009. APP expression, distribution and accumulation are altered by aluminum in a rodent model for Alzheimer's disease. J Inorg Biochem 103(11):1548–1554, PMID: 19818510, https://doi.org/10.1016/j.jinorgbio.2009.07.027.

Wright AL, Zinn R, Hohensinn B, Konen LM, Beynon SB, Tan RP, et al. 2013. Neuroinflammation and neuronal loss precede Aβ plaque deposition in the hAPP-J20 mouse model of Alzheimer's disease. PLoS One 8(4):e59586, PMID: 23560052, https://doi.org/10.1371/journal.pone.0059586.

Xu L, Zhang W, Liu X, Zhang C, Wang P, Zhao X. 2018. Circulatory levels of toxic metals (aluminum, cadmium, mercury, lead) in patients with Alzheimer's disease: a quantitative meta-analysis and systematic review. J Alzheimers Dis 62(1):361–372, PMID: 29439342, https://doi.org/10.3233/JAD-170811.

Yoon S-S, AhnJo S-M. 2012. Mechanisms of amyloid-β peptide clearance: potential therapeutic targets for Alzheimer's disease. Biomol Ther (Seoul) 20(3):245–255, PMID: 24130920, https://doi.org/10.4062/biomolther.2012.20.3.245.

Zhao Z, Xiang Z, Haroutunian V, Buxbaum JD, Stetka B, Pasinetti GM. 2007. Insulin degrading enzyme activity selectively decreases in the hippocampal formation of cases at high risk to develop Alzheimer's disease. Neurobiol Aging 28(6):824–830, PMID: 16769157, https://doi.org/10.1016/j.neurobiolaging.2006.05.001.